the plant journal

The Plant Journal (2020) 104, 76–95 doi: 10.1111/tpj.14906

Model-assisted identification of metabolic engineering strategies for *Jatropha curcas* lipid pathways

Sandra M. Correa[1,4], Saleh Alseekh[2,3], Lucía Atehortúa[4], Yariv Brotman[1,5], Rigoberto Ríos-Estepa[6], Alisdair R. Fernie[2,3] and Zoran Nikoloski[3,7,8,*]

[1]*Genetics of Metabolic Traits Group, Max Planck Institute of Molecular Plant Physiology, Potsdam 14476, Germany,*
[2]*Central Metabolism Group, Max Planck Institute of Molecular Plant Physiology, Potsdam 14476, Germany,*
[3]*Centre for Plant Systems Biology and Biotechnology, Plovdiv 4000, Bulgaria,*
[4]*Grupo de Biotecnología, Departamento de Ciencias Exactas y Naturales, Universidad de Antioquia, Medellín 050010, Colombia,*
[5]*Department of Life Sciences, Ben-Gurion University of the Negev, Beer-Sheva 8410501, Israel,*
[6]*Grupo de Bioprocesos, Departamento de Ingeniería Química, Universidad de Antioquia, Medellín 050010, Colombia,*
[7]*Bioinformatics, Institute of Biochemistry and Biology, University of Potsdam, Potsdam 14476, Germany, and*
[8]*Systems Biology and Mathematical Modelling Group, Max Planck Institute of Molecular Plant Physiology, Potsdam-Golm 14476, Germany*

Received 23 January 2020; revised 3 June 2020; accepted 12 June 2020; published online 12 July 2020.
*For correspondence (e-mail nikoloski@mpimp-golm.mpg.de).

SUMMARY

Efficient approaches to increase plant lipid production are necessary to meet current industrial demands for this important resource. While *Jatropha curcas* cell culture can be used for *in vitro* lipid production, scaling up the system for industrial applications requires an understanding of how growth conditions affect lipid metabolism and yield. Here we present a bottom-up metabolic reconstruction of *J. curcas* supported with labeling experiments and biomass characterization under three growth conditions. We show that the metabolic model can accurately predict growth and distribution of fluxes in cell cultures and use these findings to pinpoint energy expenditures that affect lipid biosynthesis and metabolism. In addition, by using constraint-based modeling approaches we identify network reactions whose joint manipulation optimizes lipid production. The proposed model and computational analyses provide a stepping stone for future rational optimization of other agronomically relevant traits in *J. curcas*.

Keywords: *Jatropha curcas*, lipid biosynthesis and metabolism, metabolic reconstruction, constrained-based analysis, cell cultures, metabolic engineering.

INTRODUCTION

Plant lipids provide essential fatty acids (FA) in the human diet and constitute a biofuel source and an alternative feedstock for the chemical industry, with their levels of production projected to double by 2040 (Bates *et al.*, 2013; Fonseca *et al.*, 2016). *Jatropha curcas*, a plant from the family Euphorbiaceae, has an untapped potential to meet the increasing demand for plant lipids (Akintayo, 2004; Maes *et al.*, 2009). Although tremendous progress has been achieved in domestication and breeding of *J. curcas*, establishment of this plant as a competitive crop remains elusive (Montes and Melchinger, 2016). An *in vitro* lipid production system based on *J. curcas* cell cultures can harness the benefits of this plant (US Patent 7 772 002 B1, 10 August 2010 and US Divisional Patent 7 968 338 B1, 28 June 2011); however, maximizing the productivity and efficiency of such a system for industrial applications necessitates understanding the effects of growth conditions on metabolism and lipid production.

The design of a strategy to manipulate *in vitro* lipid production and composition in *J. curcas*, and plants in general is hampered by the incomplete knowledge of lipid metabolic pathways, their regulation and compartmentalization within a cell, as well as their variation between cell types, developmental stages and environments (Napier *et al.*, 2014; Allen *et al.*, 2015). Flux estimation studies have attempted to bridge this gap by studying the operation and regulation of lipid metabolism in seed tissues, cell suspension cultures and intact plants from different species, including soybean (Sriram *et al.*, 2004; Allen *et al.*, 2009),

maize (Alonso *et al.*, 2010), rapeseed (Schwender and Ohlrogge, 2002; Schwender *et al.*, 2004), sunflower (Alonso *et al.*, 2007a) and Arabidopsis (Bao *et al.*, 2000; Lonien and Schwender, 2009) under different conditions. These studies have augmented our understanding of the metabolic fluxes involved in production of lipid precursors by employing labeling approaches with stable or radioactive isotopes. However, determining the reaction pathways which connect particular lipid species to precursors and intermediates, alternative pathways and their operation and regulation is far from being fully resolved.

The existing large-scale models of plant metabolism either focus on central metabolism or consider inclusion of lipid metabolic pathways based solely on gene annotation (Nikoloski *et al.*, 2015). Access to a high-quality condition-specific metabolic network for *J. curcas* with strong experimental support would facilitate the identification of metabolic reaction steps which affect the accumulation of storage lipids under different *in vitro* conditions and can be used in rational optimization of the system for industrial applications. Here we provide a bottom-up reconstruction of the metabolic network of *J. curcas* supported by labeling experiments. We used this network to characterize the distribution of fluxes under three carbon growth scenarios, and identify potential targets for increasing lipid biosynthesis at little cost to biomass production. It is important to emphasize that our focus was the metabolic flux analysis of lipid pathways, thus our study contributes knowledge about the reactions and pathways which constitute storage lipid biosynthesis in *J. curcas* as well as their operation and relation to the rest of the plant's metabolism. Therefore, our computational analysis in combination with heterogeneous data helped us identify the determinants of productivity and efficiency of a *J. curcas*-based *in vitro* system for lipid production.

RESULTS

Reconstruction of the *J. curcas* metabolic network

We generated a bottom-up reconstruction of the metabolic model of *J. curcas* supported by experimental evidence and with emphasis on resolving lipid pathways via labeling. The model consists of 800 reactions and 647 metabolites organized in eight cellular compartments (Figure 1, Data S1 in the online Supporting Information). In this manually curated reconstruction, we evaluated each reaction with respect to the *J. curcas*-specific literature and database (Jatropha Genome Database, http://www.kazusa.or.jp/jatropha/). We also used information from phylogenetically related species (e.g. *Ricinus communis*), model plant species (e.g. the Aralipid website, specifically built for *Arabidopsis thaliana*; Li-Beisson *et al.*, 2013) and studies with heterotrophic plant cells and tissues, as well as the Kyoto Encyclopedia of Genes and Genomes (KEGG), the enzyme repository BRENDA and the universal protein database (UniProt) (see Experimental Procedures). We also ensured that reactions were mass- and charge-balanced and provided support for their directionality according to the biochemical data available in the literature. In addition, diverse bibliomic data were examined to facilitate an up-to-date and accurate reconstruction and compartmentalization for storage and structural FA biosynthetic pathways in *J. curcas*. Finally, and most importantly, the findings from the isotope labeling experiments (ILEs) were also used for refinement purposes (see Experimental Procedures), a point which could not be resolved by relying solely on homology-based gene annotations.

Isotope labeling and refinement of lipid biosynthesis pathways

To ensure that the network accurately captures the lipid metabolism of *J. curcas* cells, we used the data obtained from ILEs in which we independently supplied glucose and glycerol as labeled substrates (see Experimental

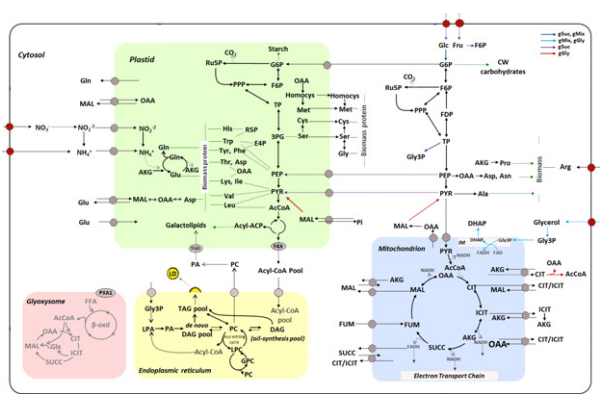

Figure 1. Scheme of central carbon metabolism and the routes for the formation of the main biomass components (i.e. proteinogenic amino acids, starch, lipids and cell wall carbohydrates).
The coloured arrows on the top-right indicate the reactions taking place in the specified growth conditions [sucrose, gSuc; glucose/glycerol, gMix; glycerol, gGly], the black arrows of the model connecting the metabolites symbolize the reactions taking place under the three growth scenarios evaluated. Key: 3-PG, 3-phosphoglycerate; AcCoA, acetyl-coenzyme A; ADPglc, ADP-glucose; AKG, alpha-ketoglutarate; Ala, alanine; Arg, arginine; Asn, asparagine; Asp, aspartate; β-oxid, β-oxidation; CIT, citrate; Cys, cysteine; CW, cell wall; DAG, diacylglycerol; DHAP, dihydroxyacetone phosphate; E4P, erythrose-4-phosphate; F6P, fructose-6-phosphate; FAX, fatty acid export; FDP, fructose diphosphate; Fru, fructose; FUM, fumarate; G6P, glucose-6-phosphate; Glc, glucose; Gln, glutamine; Glu, glutamate; Gly3P, glycerol-3-phosphate; Gly, glycine; GPC, glycerophosphocholine; Glx, glyoxylate; His, histidine; ICIT, isocitrate; Ile, isoleucine; IM, mitochondrial intermembrane space; LD, lipid droplet; Leu, leucine; LPA, lysophosphatidic acid; LPC, lysophosphatidylcholine; Lys, lysine; MAL, malate; Met, methionine; OAA, oxaloacetate; PA, phosphatidic acid; PC, phosphatidylcholine; PEP, phospho*enol*pyruvate; Phe, phenylalanine; PPP, pentose phosphate pathway; Pro, proline; PYR, pyruvate; PXA1, peroxisomal ABC-transporter; Ru5P, ribulose-5-phosphate; R5P, ribose-5-phosphate; Ser, serine; SUCC, succinate; TAG, triacylglycerol; Thr, threonine; TP, trioses phosphate; Trp, tryptophane; Tyr, tyrosine; Val, valine.

Procedures). The resulting labeling patterns of the identified lipid species (Table S1) were in turn employed to elucidate and further refine the topology of the lipid biosynthesis pathways. The labeling patterns of a species here specify its different isotopic composition, called mass isotopologue distribution. We also used the data from these experiments to estimate fluxes of reactions in lipid metabolism and some reactions in central metabolism.

Different enzymes involved in FA and lipid biosynthesis have already been identified through genomic and transcriptomic studies (Gu *et al.*, 2012; Sood and Chauhan, 2015; Ma *et al.*, 2017); therefore, it is feasible that there are several routes for storage lipid formation in Jatropha seeds. The first route considered in Jatropha cell cultures for glycerolipid assembly in the endoplasmic reticulum (ER) was the Kennedy pathway. In the context of plant lipid biochemistry, the Kennedy pathway describes the direct production of triacylglycerol (TAG) by the sequential *sn*-1, *sn*-2 and *sn*-3 acylations of the glycerol-3-phosphate backbone. The *sn*-1 acylation produces lysophosphatidic acid; this is followed by the *sn*-2 acylation to give phosphatidic acid, which in turn is converted to diacylglycerol (DAG) by the action of phosphatidic acid phosphatase (PAP). Finally, the *sn*-3 acylation produces TAG (Stymne and Stobart, 1987; Napier, 2007; Bates *et al.*, 2009). On the other hand, DAG represents an important branch point between neutral and membrane lipid biosynthesis. This implies that DAG may be acylated to produce TAG, but also that it can be converted into phosphatidylcholine (PC) by cytidine 5′-diphosphocholine (CDP-choline):1,2-diacyl-*sn*-glycerol cholinephosphotransferase (CPT) (Speerling and Heinz, 1993; Sperling *et al.*, 1993; Harwood, 1996; Bates *et al.*, 2009). The enzyme CPT is expressed in Jatropha seeds at different developmental stages (Jiang *et al.*, 2012), thus it was included as a component of the lipid network.

The isotopologue distribution data obtained through the ILEs was used to calculate the rate of decay of the non-labeled fractions of metabolites, necessary for the implementation of the kinetic flux profiling (KFP) approach (see Experimental Procedures). When no change (increase or decrease) is observed in the isotopologue distribution of a defined metabolite, we considered it as an indication that the metabolic pool is not active at the time when the ILE took place. In contrast, when a decay is observed in the non-labeled fraction (m + 0) of a metabolite, with a concomitant increase of the other isotopologues (m + 1, m + 2, m + 3, etc.), we assumed that the pool is active. When the isotopologue distribution data for all the lipid species identified in Jatropha cell samples were analyzed, we observed that some lipid pools were inactive for the entire time span of the ILEs (Table S1).

After the analysis of the obtained mass isotopologue distributions, we observed that many DAG species were not labeled, although label was incorporated in almost all PC and in most TAG species. This implies that TAG species could be derived from non-labeled DAG by attaching a labeled FA to the *sn*-3 position of the glycerol backbone. However, the content of DAG species was several orders of magnitude smaller than that of TAG species. If unlabeled DAG pools were used as a sole precursor of TAG species, they would be depleted in the course of the ILEs. However, unlabeled DAG species were detected at every measured time point and their content remained almost invariant over the time interval measured. This indicated that not all DAG pools were very likely to be used as substrates for TAG synthesis and that their *de novo* synthesis did not occur during the ILEs. Therefore, we concluded that the Kennedy pathway is not the only route for TAG synthesis in this species.

An alternative possible route for TAG synthesis is via the recycling of intermediates of membrane lipid synthesis (e.g. PC). The use of PC-derived DAG has been proposed as the major pathway for TAG synthesis in *Linum usitatissimum* and *Glycine max* (Slack *et al.*, 1978; Bates *et al.*, 2009). Based on the findings from the ILEs and the number and type of lipid species identified, we argue that at least three mechanisms can contribute to TAG synthesis in Jatropha cells: (i) the above-mentioned synthesis of TAG through the Kennedy pathway, (ii) the synthesis of TAG from PC-derived DAG, with the participation of acyl-CoA as the acyl donor and (iii) the acyl-CoA-independent mechanism where DAG can be acylated to form TAG, with the participation of phospholipids (e.g. PC) as acyl donors, in a reaction catalyzed by the enzyme phospholipid:diacylglycerol acyltransferase (PDAT) (Dahlqvist *et al.*, 2000; Zhang *et al.*, 2009; Li-Beisson *et al.*, 2013). As a result, the total DAG pool could be divided into sub-pools (Figure 2): The first DAG sub-pool was synthesized prior to the ILEs and remained inactive during the ILEs (due to the concluded partial inactivity of the Kennedy pathway). The second DAG sub-pool was subsequently formed by labeled DAG species which act as precursors to several *de novo* synthesized PC labeled species. The interconversion of DAG and PC is already a firmly established mechanism in oilseed metabolism (Slack *et al.*, 1983; Triki *et al.*, 1999; Bates *et al.*, 2009). The third DAG sub-pool, namely the DAG oil-synthesis pool, is composed of the PC-derived DAG directed to TAG synthesis (Bates *et al.*, 2009). We assumed that DAG and PC pools were not at equilibrium since the composition of labeled species in the DAG and PC pools differed (Figure 2).

The expression of the gene coding for PDAT has been reported in Jatropha seeds at certain developmental stages (Costa *et al.*, 2010; Xu *et al.*, 2011; Jiang *et al.*, 2012; Sood and Chauhan, 2015; Ha *et al.*, 2019). However, the activity of PDAT alone is not enough to justify all the labeled TAG species detected, since the participation of both DAG and PC pools is essential for its activity. Phospholipase C (PLC)

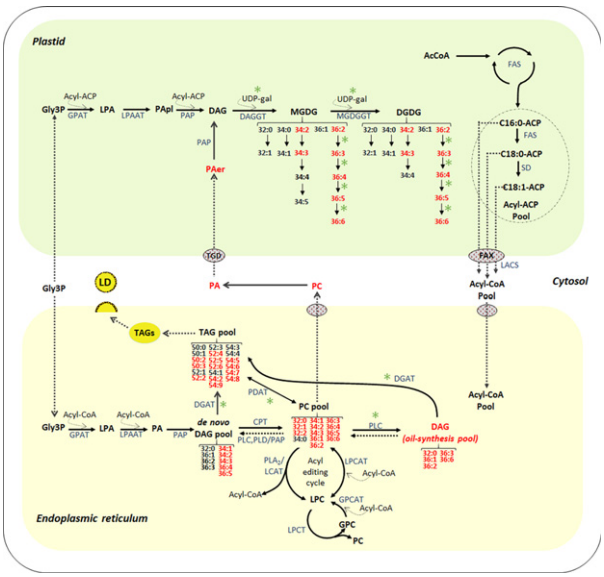

Figure 2. Simplified scheme of the lipid biosynthetic network for *in vitro Jatropha curcas* cells.
In plastids, the main steps of fatty acid synthesis are included. In the same compartment, the route of galactolipid formation and the mechanism for their unsaturation are outlined. In the endoplasmic reticulum (ER) the routes for glycerolipid and lipid droplet formation are included. Labeled lipid species are displayed in red letters and reactions whose fluxes were estimated by following the kinetic flux profiling approach are identified with a green asterisk. Key: CPT, CDP-choline:1,2-diacyl-snglycerol cholinephosphotransferase; DAGGT, UDP-alpha-D-galactose:1,2-diacyl-*sn*-glycerol 3-beta-Dgalactosyltransferase; DGAT, diacylglycerol acyltransferase; GPAT, acyl-CoA: *sn*-glycerol-3-phosphate acyltransferase; FAS, fatty acid synthase; GPC, *sn*-glycero-3-phosphocholine; GPCAT, acyl-CoA:glycerophosphocholine acyltransferase; LACS, long-chain acyl-CoA synthetase; LCAT, phosphatidylcholine-sterol *O*-acyltransferase; LPAAT, acyl-CoA: lysophosphatidic acid acyltransferase; LPCT, lysophosphatidylcholine transacylase; MGDGGT, UDP-alpha-D-galactose:1,2-diacyl-3-beta-D-galactosyl-*sn*-glycerol 6-alpha-D-galactosyltransferase; PAer, phosphatidic acid, ER-derived; PApl, phosphatidic acid, plastid-derived; PAP, phosphatidic acid phosphatase; PDAT, phospholipid:diacylglycerol acyltransferase; PDCT, phosphatidylcholine diacylglycerol cholinephosphotransferase; PLA2, phospholipase A2; PLC, phospholipase C; PLD, phospholipase D; UDP-gal, UDP-galactose.

is an enzyme with hydrolase activity that cleaves the choline moiety from PC, releasing DAG and phosphocholine. The expression of the gene coding for PLC has been reported in developing Jatropha endosperm (Gu *et al.*, 2012), hence the hydrolytic reaction catalyzed by PLC together with the activity of acyl-CoA:diacylglycerol acyltransferase (DGAT) was included in the reconstruction. In the model, the activity of PDAT, PLC and DGAT accounted for the use of PC pools and PC-derived DAG for TAG synthesis. Descriptions for the likely topology of the TAG synthesis pathway for Jatropha cells *in vitro* are summarized in Figure 2.

According to the labeling pattern of the PC species in Jatropha cells, we propose that in addition to the *de novo* PC synthesis via the precursor DAG, the route of PC re-synthesis via lysophosphatidylcholine may also be operational. This is a route that does not require the degradation of glycerophosphocholine into free choline, the activation of choline to CDP-choline, or the utilization of CDP-choline by CDP-choline:diacylglycerol cholinephosphotransferase (Van der Rest *et al.*, 2002; Lager *et al.*, 2015) (Figure 2). We identified several highly unsaturated species in the PC pool, probably generated from the *de novo* synthesized PC. This is supported by the fact that PC is the major site for the eukaryotic FA desaturation pathway and related reactions (Sperling *et al.*, 1993; Bates *et al.*, 2009), whereas evidence for a direct role of DAG or TAG as a desaturase substrate is still lacking. The mechanisms of acyl editing were also included to account for the highly unsaturated acyl chains detected for some lipid species (Lands, 1965; Stymne and Stobart, 1984; Shindou and Shimizu, 2009). The route of galactolipid formation, including the likely origin of precursors and the pattern of desaturation, was proposed according to the labeling data for the identified galactolipid species, and is also based on the well-established mechanisms reported by Harwood, (1996) (Figure 2).

The points about stitching the lipid pathways together based on the labeling patterns and established knowledge further demonstrate that reconstruction of the pathway based solely on annotated gene functions would have resulted in inaccuracies in the model reconstruction and inconsistencies with respect to the generated data sets.

Verification of the metabolic (quasi)steady state and condition-specific growth profiles, substrate consumption and biomass composition

Employing different methodological and analytical tools, we next gathered condition-specific experimental data from Jatropha cells grown on different carbon sources. Growth profiles of cells with the distinct growth phases were measured by quantifying substrate consumption and dry biomass weight. We estimated exchange fluxes by using data on assimilation of carbon sources and inorganic ions (Table S2).

We also measured cell growth to determine the time interval during which metabolism can be assumed to be at metabolic (quasi)steady state, which is essential for modeling (Wiechert, 2001). In plant cell cultures, central metabolism is highly stable during the exponential growth phase, whereby the flux values of the participating reactions remain constant. Changes in fluxes start to occur only when the growth rate of the cell culture declines, typically occurring during the transition from the exponential to the stationary growth phase (Rontein *et al.*, 2002; Williams *et al.*, 2008; Kruger *et al.*, 2012). This has also been the approach employed to assess the metabolic (quasi)steady state for metabolic flux analysis with yeast and bacteria in batch and fed-batch culture (Nielsen *et al.*, 2003; Ghosh *et al.*, 2016; Zhang *et al.*, 2016). For each

condition, we identified the time lapse of the exponential growth phase when cells are growing at a constant and maximum rate, which spanned from 4 to 8 days in sucrose (gSuc) and 5–10 days for glucose and glycerol (gMix) and glycerol (gGly).

The assumption of a metabolic steady state was additionally verified by three sets of experiments. In the first set, 10 metabolic intermediates of glycolysis were quantified during a time lapse spanning the exponential growth phase of gSuc (days 4–12). Using a one-way analysis of variance in all cases we were unable to identify any significant differences ($\alpha = 0.05$) in the concentration of each of the 10 measured metabolites between days 4 and 12 (Table S3).

In the subsequent set of experiments, soluble metabolic intermediaries were measured. A total of four, five and six metabolites were quantified in gSuc, gMix and gGly, respectively. We could not identify significant differences for any of the metabolic pools evaluated ($\alpha = 0.05$) (Table S3). In the last set of experiments, a total of 23, 23 and 26 lipid pools were measured in gSuc, gMix and gGly, respectively. In this case, too, we did not detect any significant differences in the metabolite levels between days 5 and 8 in gSuc ($\alpha = 0.05$) and days 7 and 9 in gMix and gGly (Table S3). Taken together, we concluded that during the exponential growth phase the metabolic steady state holds for the three growth conditions during the time lapse when the ILEs were performed.

Furthermore, we characterized the biomass composition for cells grown on the different carbon sources (Table S4, Figure 3a). Cells grown on sucrose accumulated more protein (41% w/w) than starch (30% w/w), while cells grown on the glucose and glycerol mixture showed the opposite pattern, i.e. 35% w/w starch and 26% w/w protein. When cells were grown on glycerol, protein accounted for the largest percentage (49% w/w), while starch constituted a small proportion (18% w/w). The remaining components (i.e. lipids and cell wall carbohydrates) had modest and similar contributions in all cases. Using the experimental data obtained from the biomass characterization procedure, three condition-specific biomass reactions were then constructed. The model reconstruction procedure ensured that reactions necessary for the biosynthesis of all necessary metabolite precursors were included.

Simulation and validation of cell growth and fluxes in lipid biosynthesis pathways

The constructed models of condition-specific biomass production were subsequently used to simulate growth based on flux balance analysis (FBA) (Thiele and Palsson, 2010; Schellenberger *et al.*, 2011). Without constraining the substrate consumption rates, the condition-specific growth predicted by the model, setting biomass production as the objective function resulted in unrealistically high prediction of growth. However, sequential inclusion of constraints for

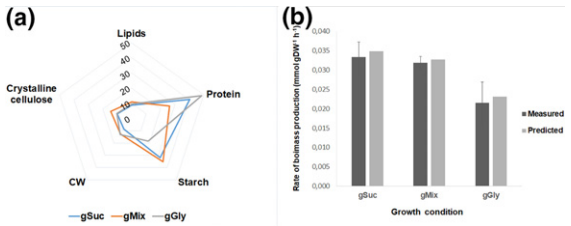

Figure 3. Biomass characterization under three different growth conditions.
(a) Differences in biomass composition (% w/w) in *Jatropha curcas* cells growing on three carbon sources [i.e. sucrose (gSuc), glucose and glycerol (gMix), and glycerol (gGly)]. CW, cell wall carbohydrates.
(b) The rate of biomass production obtained from experimental measurements and from model prediction for cells growing on different carbon sources. Error bars display the standard deviation.

rates of carbon, nitrogen, sulfur and phosphate consumption, the condition-specific biomass reactions, the KFP-estimated fluxes and the maintenance constraints resulted in quantitatively excellent predictions for each growth condition (Figure 3b).

Using the data from the ILEs we estimated the fluxes of 23, 16 and 21 reactions based on the KFP (Yuan *et al.*, 2008) in gSuc, gMix and gGly, respectively (Table S6, Figure 2). We observed differences in the order of magnitude of the experimentally estimated fluxes, where fluxes from central metabolism were several orders of magnitude larger than fluxes from lipid pathways. This difference in the order of magnitude has also been observed in other organisms (e.g. bacteria and yeast). The work done by Almaas *et al.* (2004) led to the observation that flux distribution follows a power law, which implies that most metabolic reactions exhibit small fluxes while the biochemical activity of the metabolism is controlled by several reactions with very high fluxes, leading to the concept of a high-flux backbone in metabolic networks (Almaas *et al.*, 2004; Samal, 2008). In addition, we must also stress that lipids are big molecules compared with other intermediates of central metabolism in terms of the number of carbon units required to build 1 mol of a lipid molecule (e.g. TAG, DAG, PC), thus fluxes from central metabolism feeding lipid biosynthesis pathways are expected to be considerably larger.

In addition, we used all experimentally derived constraints, including the exchange fluxes as well as the non-growth-associated maintenance (NGAM) values, to predict fluxes at the point of optimum condition-specific growth (setting condition-specific biomass synthesis as the objective function) followed by total flux minimization (Experimental Procedures). While in all cases the fluxes estimated from the data were larger than flux predictions from the constrained model, they were highly correlated (Pearson correlation coefficient >0.86) in the three conditions (Table S7). The estimated fluxes of some reactions showed

higher deviation from the best fit with respect to the predicted value; a typical example is the reactions in galactolipid synthesis. Since galactolipids are membrane constituents, part of their pool may be inactive, thus contributing to a delay in the decay of the unlabeled fraction used in KFP, leading to the discrepancy in the flux estimation. As an additional validation of the flux estimates, incorporation of KFP-estimated fluxes in the simulation of growth provided a further improvement of the fit for gSuc and gMix and did not affect the predictions for the gGly condition.

Differential flux profiling, energy metabolism, and reducing power generation

We next used all constraints, including the KFP-estimated fluxes, and performed flux variability analysis (FVA) under optimum condition-specific growth to conduct differential flux profiling (Experimental Procedures). To this end, we categorized each reaction based on the number of pairwise condition comparisons in which the corresponding flux intervals did not overlap. We found that the ranges of 259 reactions differed between all three pairwise condition comparisons, while 79 and 57 showed differences in two and single pairwise condition comparisons, respectively (Table S8). This finding indicated that there is a large amount of flux rerouting between the three growth conditions.

Furthermore, after the use of the KFP-estimated fluxes as constraints, we determined a reduction of up to 77.9%, 69.7% and 66.0% in the feasible range for 623, 558 and 528 of the reactions for the gSuc, gMix and gGly conditions, respectively (Table S9). These flux ranges were used to characterize the major differences in flux distributions between the growth conditions: in all growth conditions, glycolysis was predicted to operate in both cytosol and plastids. In gMix and gGly, the model predicted that the reaction catalyzed by the cytosolic fructose diphosphate aldolase was operating in a reverse mode, while fructose-1,6-biphosphatase was active. This could be explained by the need to replenish fructose-6-phosphate and glucose-6-phosphate (G6P) pools, because externally supplied glucose could partially meet the demands for these intermediates in gMix and is not externally supplied in gGly (Figure 1). In addition, the model predicted a full operation of the cytosolic and plastidial pentose phosphate pathway (PPP) in all growth conditions. The model predicted that in gSuc, gMix and gGly the intermediates imported into the plastids included G6P, oxaloacetate and phospho*enol*pyruvate, besides pyruvate in gSuc and malate in gGly.

We next employed the experimental data and the estimated NGAM costs to evaluate the distribution of reducing power generation in the different cell compartments. In the metabolic reconstruction there were several redox shuttles, whose contributions were considered when calculating the reducing power generation in the different cellular compartments:

i A redox shuttle of proline metabolism, which is transported from the cytosol to the mitochondrion, where the electrons from proline are transferred to the FAD cofactor to produce FADH, and from there to a quinone acceptor. The pyrroline-5-carboxylate intermediate produced in this reaction is further metabolized by the enzyme pyrroline-5-carboxylate dehydrogenase to produce glutamate with the concomitant generation of one molecule of NADH (Di Martino *et al.*, 2006; Planchais *et al.*, 2014). This is part of a route that modulates the content of basic amino acids in plant cells.

ii A redox shuttle of isocitrate metabolism, where several mitochondrial carriers export isocitrate to the cytosol (Haferkamp, 2007; Linka and Weber, 2009). The isocitrate is in turn metabolized by the activity of isocitrate dehydrogenase (ICDH) enzymes, two of which are located in the mitochondrion and one in the cytosol to produce 2-oxoglutarate (OG). The interconversions between isocitrate and OG represents a flexible mechanism in which the ICDH enzymes are involved in the maintenance of the metabolic balance between reduced and oxidized pyridine nucleotides (Igamberdiev and Gardeström, 2003).

iii A redox shuttle of malate metabolism, where NADP-malic enzyme, a widely distributed enzyme, catalyzes the oxidative decarboxylation of malate to yield pyruvate, CO_2 and NADPH. There exist plastidial and cytosolic isoforms of this enzyme, which contribute with carbon and reducing power for FA synthesis and FA elongation, respectively. The mitochondrion is source for the malate used as substrate by this enzyme, exported through well-known carriers (Drincovich *et al.*, 2001; Pleite *et al.*, 2005).

In gGly we estimated the highest generation of FADH and NADH (0.3036 and 0.4611 mmol gDW^{-1} h^{-1}, respectively; DW, dry weight), followed by FADH production in gMix (0.2185 mmol gDW^{-1} h^{-1}) and NADH in gSuc (0.1587 mmol gDW^{-1} h^{-1}). Production of NADPH was predicted to be higher in gMix (0.7691 mmol gDW^{-1} h^{-1}), followed by gSuc and gGly (0.5724 and 0.4904 mmol gDW^{-1} h^{-1}, respectively) (Table S5). The contribution of the compartments (i.e. mitochondrion, cytosol and plastids) also varied across conditions. In gSuc, around 69% of the total reducing power was generated in the cytosol, while 25% and 6% was produced in the plastids and mitochondrion, respectively. In gMix the contribution of mitochondrion, cytosol and plastids was 22%, 19% and 59%, respectively, and in gGly the numbers were 50%, 8% and 42%, respectively (Table S5). These differences might be due to the differential biomass composition, the need to cope with the NGAM requirements as well as the medium composition, especially the carbon source

supplied: in gGly and gMix, with glycerol as a carbon source, the reaction catalyzed by FADH-dependent glycerol-3-phosphate dehydrogenase taking place in the mitochondrial intermembrane space was predicted to make a large contribution to reducing power generation (Figure 1, Table S5).

Identification of overexpression targets affecting storage lipid accumulation and composition

To identify reactions whose overexpression would be anticipated to increase storage lipid accumulation, we made use of the FSEOF ('flux scanning based on enforced objective flux') approach (Choi *et al.*, 2010). To this end, we investigated two target reactions that were of particular interest to us: the lipid body formation (LBF) reaction, modeling the accumulation of storage lipids (i.e. TAGs) in the organelles known as lipid bodies or lipid droplets, and the reaction catalyzed by stearoyl-ACP-desaturase (SACPD), synthesizing oleic acid (C18:1), to obtain storage lipids enriched in this particular FA. To constrain the target reactions we made use of an algorithm that constrained the reactions to their calculated, theoretical maximum values, and then proceeded to obtain the respective flux distributions. When the flux distribution was not feasible at maximum growth, the algorithm made a gradual reduction of the respective values used as constraints until a feasible flux distribution was achieved (Experimental Procedures). The fluxes of the target reactions were thus constrained in each condition without sacrificing biomass production, as our goal was to achieve the maximum lipid accumulation without reducing the biomass yield. We then identified reactions with an increased flux with respect to the reference. For all three growth conditions, the reactions with increased flux were classified into subsystems (Experimental Procedures).

After constraining the SACPD and LBF reactions, we observed that some biomass components (i.e. galactolipids, amino acids and cell wall components) were favored for all the scenarios evaluated, as the fluxes leading to their synthesis were increased compared with the respective reference flux distribution. The fluxes of reactions leading to the synthesis of several cell wall components were larger than the respective reference flux distributions, as was the case for reactions of galacturonic acid, xylose and GDP-glucose synthesis in gMix and gGly, besides reaction for galactose synthesis in gGly. In gSuc, the reactions for rhamnose and fucose (also present in gMix) synthesis were identified. The reactions for starch synthesis had increased fluxes only in gGly (Table S10, Figures 4b and 5).

In all growth conditions the amino acid reactions that showed an increased flux were related to the synthesis of lysine, methionine, serine, leucine, valine, isoleucine and threonine. In addition, the reactions for phenylalanine, tyrosine, tryptophan and cysteine synthesis in gSuc, the reactions for histidine, glutamate and proline synthesis in gMix, and proline synthesis in gGly also increased. The correlation between the increase in lipid-related reaction fluxes and the fluxes of amino acid-related reactions is analogous to the observations made by Borisjuk *et al.* (2013) in rapeseed embryos, as they noticed the simultaneous occurrence of lipid and protein storage accumulation as part of the tissue differentiation program. During these events, there is competition among the biosynthetic pathways for the same substrates and energy, and the evidence suggests that redirection of substrates from lipid to protein synthesis is feasible (Chen *et al.*, 2009; Borisjuk *et al.*, 2013), while the opposite has proven more difficult to engineer (Abbadi and Leckband, 2011; Borisjuk *et al.*, 2013). Our study shows that the increased flux in reactions of amino acid and cell wall component synthesis might be an indirect consequence of the increased accumulation of storage lipids enriched in a particular FA. The latter leads to activation of the lipid degradation pathways, resulting in the likely higher availability of metabolic intermediates that are redirected to other biomass components. This is also in line with the evidence from breeding programs where selection for total content of protein and lipid has been

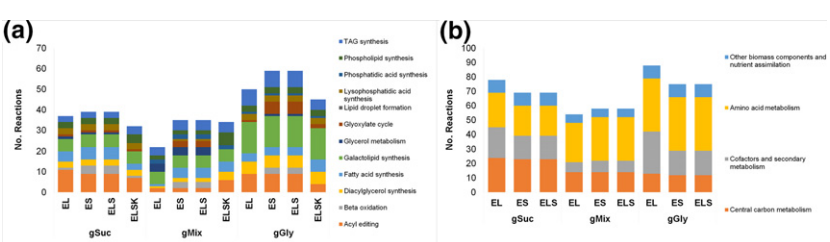

Figure 4. Optimization of storage lipid accumulation by reaction manipulation.
(a) Number of reactions related to lipid synthesis displaying increased flux upon flux scanning based on enforced objective flux (FSEOF) under four different constraint scenarios: EL, constraints only on the lipid body formation (LBF) reaction; ES, constraints only on the stearoyl-ACP-desaturase (SACPD) reaction; ELS, combined constraints on LBF and SACPD; ELSK, consideration of knock-out of β-oxidation reactions. Reactions are categorized into subsystems.
(b) Reactions categorized into main functional categories: central carbon metabolism, amino acid metabolism, generation of biomass components, cofactors, and secondary metabolism, displaying increased flux under the four different constraint scenarios. DAG, diacylglycerol; FA, fatty acid; LPA, lysophosphatidic acid; PA, phosphatidic acid; PL, phospholipid.

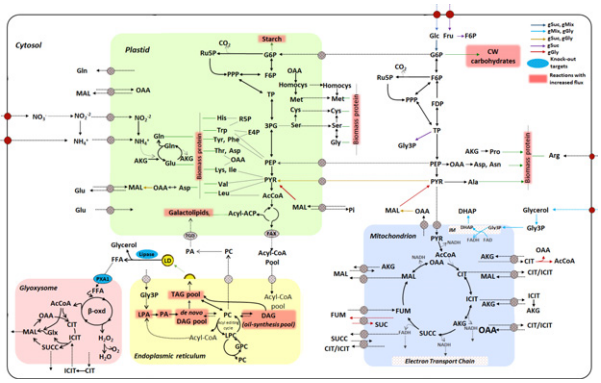

Figure 5. Scheme of central carbon metabolism and the routes for the formation of the main biomass components (i.e. proteinogenic amino acids, starch, lipids, and cell wall carbohydrates) upon flux scanning based on enforced objective flux (FSEOF) implementation.
The coloured arrows on the top-right indicate the reactions taking place in the specified growth conditions [i.e. sucrose (gSuc), glucose and glycerol (gMix), and glycerol (gGly)], the black arrows of the model connecting the metabolites symbolize the reactions taking place under the three growth scenarios evaluated. The reaction steps enclosed in the blue circles correspond to the knock-out targets in the FSEOF analysis. The biomass components enclosed in the red boxes are associated with reactions related to their biosynthetic pathways that showed increased fluxes under the scenarios of high lipid accumulation. 3-PG, 3-phosphoglycerate; AcCoA, acetyl-coenzyme A; ADPglc, ADP-glucose; AKG, alpha-ketoglutarate; Ala, alanine; Arg, arginine; Asn, asparagine; Asp, aspartate; β-oxid, β-oxidation; CIT, citrate; Cys, cysteine; CW, cell wall; DAG, diacylglycerol; DHAP, dihydroxyacetone phosphate; E4P, erythrose-4-phosphate; F6P, fructose-6-phosphate; FAX, fatty acid export; FDP, fructose diphosphate; FFA, free fatty acids; Fru, fructose; FUM, fumarate; G6P, glucose-6-phosphate; Glc, glucose; Gln, glutamine; Glu, glutamate; Gly3P, glycerol-3-phosphate; Gly, glycine; GPC, glycerophosphocholine; Glx, glyoxylate; His, histidine; ICIT, isocitrate; Ile, isoleucine; IM, mitochondrial intermembrane space; LD, lipid droplet; Leu, leucine; LPA, lysophosphatidic acid; LPC, lysophosphatidylcholine; Lys, lysine; MAL, malate; Met, methionine; OAA, oxaloacetate; PA, phosphatidic acid; PC, phosphatidylcholine; PEP, phospho*enol*pyruvate; Phe, phenylalanine; PPP, pentose phosphate pathway; Pro, proline; PYR, pyruvate; PXA1, peroxisomal ABC-transporter; Ru5P, ribulose-5-phosphate; R5P, ribose-5-phosphate; Ser, serine; SUCC, succinate; TAG, triacylglycerol; Thr, threonine; TP, trioses phosphate; Trp, tryptophane; Tyr, tyrosine; Val, valine.

shown to be more effective in raising lipid content than selection for lipid content alone (Grami *et al.*, 1977; Borisjuk *et al.*, 2013) (Table S10, Figure 4b).

The simulation also predicted the activation of several glyoxylate cycle, β-oxidation and glycerol metabolism reactions (acting on storage lipid degradation), not carrying flux in the reference flux distributions. These reactions were negatively correlated to SACPD according to the results from flux coupling analysis (FCA) and analysis of uniform sampled flux distributions (Table S11). The initial step of lipid breakdown is catalyzed by lipases, releasing the acyl chains from the TAGs stored in the lipid droplets (here resembling the LBF reaction) located in the cytosol, yielding free FA and glycerol (Huang, 1983; Quettier and Eastmond, 2009; Li-Beisson *et al.*, 2013). Glycerol is metabolized to the glycolytic intermediate dihydroxyacetone-phosphate by the sequential action of the enzymes glycerol kinase and the FAD-dependent glycerol-3-phosphate dehydrogenase, in the cytosol and the mitochondrial inner membrane, respectively (Eastmond, 2004; Quettier and Eastmond, 2009; Ma *et al.*, 2017). Dihydroxyacetone-phosphate is then converted into sugars by the process of gluconeogenesis. Free FA are transported to the glyoxysome (a specialized peroxisome) and activated to form acyl-CoA. Subsequently, acyl-CoAs are catabolized through the β-oxidation pathway to give raise to acetyl-CoA units which later enter the glyoxylate cycle, where several metabolic intermediates are formed (i.e. citrate, succinate, malate) and exported to other cellular compartments to fuel different reactions from central carbon metabolism (Beevers, 1980; Graham, 2008) (Figure 5).

The number of lipid degradation reactions was small or zero when LBF was constrained to values near its theoretical maximum (Figure 4a, Table S10), but the number of active β-oxidation reactions increased when the formation of C18:1 by SACPD was constrained, as was the case for the scenario where LBF and SACPD were jointly constrained. Among the active lipid degradation reactions we can name the preferential activity of lipases over TAG species with a high number of unsaturations, such as 54:3- and 54:4-TAG, which contain three and two C18:1-FA molecules, respectively; the transport reactions of C18:1-FA species to the glyoxysome; and the group of reactions of β-oxidation participating in the catabolism of C18:1-CoA to acetyl-CoA units (Table S10, Figure 4a). From the group of glyoxylate cycle reactions activated upon SACPD enforcement, we can mention the glyoxysome-localized reactions catalyzed by the enzymes isocitrate dehydrogenase, catalase, malate synthase and malate dehydrogenase. These results indicated that an increased flux through an individual reaction of FA synthesis (e.g. oleic acid formation catalyzed by SACPD) activates the routes of storage lipid degradation, and that the metabolic resources generated through degradation pathways are rerouted to other biomass components. This observation was made after manipulating lipid composition in plants, where an inadequate incorporation of FA into TAG occurs due to: (i) unbalanced activity among the block of reactions generating the FA and the block of reactions of glycerolipid assembly, or (ii) poor affinity of the acylating enzymes for their acyl-CoA substrates, turning out into the recycling of the FA via β-oxidation, even in plant tissues primarily devoted to the accumulation of storage lipids (Napier *et al.*, 2014; Poirier *et al.*, 1999; Van De Loo *et al.*, 1995).

An increased flux was also observed in reactions of several pathways of central metabolism, such as oxidative phosphorylation, the PPP, the tricarboxylic acid (TCA) cycle and the glycolysis/gluconeogenesis pathway, perhaps as a consequence of the extra availability of intermediates from the lipid degradation pathways and the need to cope with

the augmented demand for precursors for the synthesis of lipids (Table S10, Figure 4b).

For the reactions classified in the category of lipid synthesis, we observed that the number of TAG synthesis reactions with increased flux was four and five in gMix when LBF and SACPD were separately constrained, respectively. Eight reactions were of increased flux when SACPD and LBF were separately constrained in gGly, and in gSuc the number of reactions was three for both scenarios (Table S10, Figure 4a). This indicated that overexpression of SACPD alone could lead to an increase in oleic acid formation, but this does not necessarily imply a higher flux through storage lipid reactions. Taking a closer look at the identity of the TAG synthesis reactions, we noticed that in gSuc around 75% of the enzymes were acylating C18:1-FA into the glycerol backbone, while in gMix and gGly this percentage was 43%. The remaining reactions acylated C18:2-FA and C18:3-FA, probably as a result of the higher abundance of C18:1, as this later constitutes a substrate for the acyl editing mechanism generating highly unsaturated FA species. The acyl editing reactions in turn displayed an increased flux in the scenarios evaluated. Reactions producing DAG molecules were also increased, where in 33% of the reactions C18:1-acyl molecules were acylated into the glycerol backbone in gSuc, 57% in gGly and 100% in gMix (Table S10, Figure 4a).

Several galactolipid synthesis reactions also displayed increased flux in all growth conditions, especially those leading to C34 and C36 mono- and di-galactosyldiacylglycerol species, which contain one and two C18:1-FA molecules, respectively; this could be a way to re-route the C18:1 surplus (Table S10, Figure 4a).

In the pathway of FA synthesis there were also increased fluxes in several reactions, besides the obvious SACPD target reaction. Among these, we single out the fatty acid synthase complex (FAS), the heteromeric acetyl-CoA carboxylase (HetACCase) and also alternative routes for the generation of precursors and/or reducing power (i.e. malic enzyme, malate dehydrogenase and ATP-citrate lyase), which have been reported to be sources of carbon and/or reducing power in oilseeds (Pleite *et al.*, 2005; Alonso *et al.*, 2007a, 2010; Baud and Lepiniec, 2010) (Table S10, Figure 4a).

Our constraint-based modeling analysis also provided non-obvious insights about the interactions of lipid metabolism with other pathways. Borisjuk *et al.* (2013) and Hayden *et al.* (2011) highlighted the importance of certain cofactors in the storage capacity for both lipids and proteins, and suggested that the repertoire of networks regulating carbon partitioning into oil should also consider cofactor metabolism. In our study we found that reactions leading to the synthesis of some cofactors were either not active or displayed a lower flux value in the reference flux distribution, but after constraining SACPD and/or LBF, the fluxes were increased or the reactions became active. In all growth conditions, the reactions participating in the synthesis of S-Adenosylmethionine (SAM), FAD, ADP, and cytidine 5′-triphosphate cofactors were positively correlated to storage lipid accumulation. In gSuc and gGly we identified additional reactions related to the synthesis of tetrahydrofolate (THF), 5-methyltetrahydrofolate (MTHF), CoA, guanosine 5′-di- and tri-phosphate (GDP and GTP) and NADP cofactors (Table S10, Figure 4b). Some of the intermediates necessary for the synthesis of cofactors are also shared with the pathways of amino acid synthesis. For instance, these included: acetyl-L-serine, an intermediate necessary for the synthesis of cysteine and CoA; homoserine, which is intermediate in the synthesis of methionine and SAM; chorismate, an intermediate in the synthesis of THF and tryptophan. There are other reactions related to amino acids that showed an increased flux, as was the case for proline synthesis, given the redox shuttle of proline metabolism taking place in the mitochondrion; the reactions of glutamate synthesis that take part of the glutamine synthetase–glutamate synthase cycle, necessary for inorganic nitrogen assimilation; and the reactions where serine and SAM participate as substrates in the synthesis of phosphocholine that is required for phospholipid synthesis (i.e. PC) (Table S10, Figure 4b).

According to the simulation results, we identified four groups of obvious target reactions that influence storage lipid accumulation and composition in Jatropha cell cultures.

i Reactions responsible for FA synthesis (i.e. HetACCase and FAS, in addition to SACPD), whose overexpression might lead to an increased availability of FA for storage lipid assembly.

ii The TAG synthesis reactions encompassing all the steps for glycerolipid assembly [i.e. acyl-CoA: lysophosphatidic acid acyltransferase (LPAAT), DGAT and PDAT], where the purpose of their overexpression is to increase the sink strength and promote storage lipid accumulation. Here we would like to stress that, according to the results, the acylating enzymes favored the accumulation of C18:1-FA; thus, to increase the sink strength it is necessary to consider not only a higher activity of the acylating enzymes but also their affinity for the FA substrates when the goal is to produce lipids enriched with a particular FA. The overexpression of acylating enzymes with low affinity for a specific FA might lead to either the activation or an increased activity of the lipid degradation pathways, or its redirection to other lipid species (i.e. galactolipids, phospholipids) to sequester the surplus, as was observed in our analysis where a considerable number of galactolipid reactions displayed increased flux (Figure 4a, Table S10). A similar situation has been observed in attempts to alter lipid composition in oleaginous species as a result of

the regulatory mechanism of lipid homeostasis that compensates for alterations in FA composition (Napier and Graham, 2010; Napier *et al.*, 2014; Poirier *et al.*, 1999; Van De Loo *et al.*, 1995). Although the affinity of acylating enzymes has not been a major obstacle in the attempts to boost the accumulation of common FA into the storage lipids of oleaginous species (Harwood and Russell, 1984; Dörmann *et al.*, 2000; Stoutjesdijk *et al.*, 2000; Liu *et al.*, 2002, 2017; Jiang *et al.*, 2017; Morineau *et al.*, 2017), it is considered as a key aspect for evaluation in the engineering of plants to accumulate uncommon FA species (Durrett *et al.*, 2010; van Erp *et al.*, 2011, 2015; Reynolds *et al.*, 2015, 2017; Bansal *et al.*, 2018; Lunn *et al.*, 2019).

iii The LBF reactions, representing the final steps of lipid droplet formation. Lipid droplets are formed by a phospholipid monolayer, surrounded by several types of proteins, with oleosins as one of the most abundant. Increasing their availability has been demonstrated to favor lipid accumulation in plant cells as also contributes to increasing the sink strength (Siloto *et al.*, 2006; Parthibane *et al.*, 2012; Jacquier *et al.*, 2013; Winichayakul *et al.*, 2013; El Tahchy *et al.*, 2017; Xu *et al.*, 2019).

iv The last group is composed of β-oxidation reactions. Based on the FSEOF approach, we found that over-production of oleic acid was compensated by an increased flux through lipid catabolic reactions related to β-oxidation and the glyoxylate cycle. When LBF and SACPD were constrained jointly to values near their theoretical maximum, lipid catabolic reactions still exhibited increased fluxes. This indicated that increasing the flux in reactions that act further down the TAG biosynthetic pathway, to provide increased sink strength, might not be sufficient to prevent FA degradation when reactions for FA synthesis are overexpressed individually (Thelen and Ohlrogge, 2002); thus, the knock-out strategy might also be necessary to reach the desired FA composition in the storage lipids.

The previous results were also supported by FCA and analysis of uniform sampled flux distributions. Results from flux sampling in all three conditions indicated that reactions from β-oxidation, the glyoxylate cycle and TAG hydrolysis by lipases were negatively correlated to SACPD and LBF (Table S11). In addition, reactions from glycolysis, PPP, FA synthesis, lipid droplet formation and TAG synthesis were positively correlated (Table S11), supporting the overexpression targets obtained based on the FSEOF approach.

Altogether, the identified targets could be used in an integral modification strategy to optimize lipid production with the desired FA composition, following the 'push, pull and protect' strategy (Harwood and Guschina, 2013; Yuan and Grotewold, 2015; Bates, 2016).

The results of FSEOF were further scrutinized to identify other possible targets. We identified reactions related to the assimilation of nutrients (e.g. nitrate and sulfate) and other reactions with a non-obvious relation to lipid pathways (e.g. acetate, ferredoxin, purine and pyrimidine metabolism) (Table S10) besides the previously mentioned cofactors, probably pointing at inherent trade-offs between lipid metabolism and other parts of cellular metabolism.

DISCUSSION

Despite the interest in *in vitro* and field cultivation of *J. curcas* for second-generation biofuel production, there has been little effort to understand the connection between its metabolism and lipid composition, as well as yield, as agronomically relevant traits (Sood and Chauhan, 2015). Large-scale models of metabolism analyzed with approaches from constraint-based modeling can be used to get insights in the mode of operation of metabolism under different conditions and the design of intervention strategies. The quality and feasibility of these model predictions depends on the quality of the network reconstruction, improved by iterative consideration of heterogeneous molecular and physiological data. We provided a first bottom-up evidence-based metabolic reconstruction for *J. curcas* cells and refined it with data on condition-specific biomass composition and from labeling experiments with different carbon sources. Our computational analyses demonstrated that the model provides accurate quantitative and qualitative predictions of condition-specific growth and of intracellular fluxes in lipid metabolism, respectively, and can thus be used as tool to study the optimization of lipid production. The model also allowed us to pinpoint the differential operation of metabolic pathways under three conditions differing in the carbon source used. These analyses went beyond identifying the differences in precursor generation, typically obtained in seminal labeling studies in different plant species. In addition, by using three approaches from the constraint-based modeling framework we determined reactions whose overexpression or knockout can lead to increase storage lipid accumulation under *in vitro* conditions without sacrificing biomass. The identified strategy provides the means for optimization of lipid production for future industrial applications.

Although the levels of accumulation of storage lipids and the environmental conditions differed between Jatropha cell cultures and field-grown plants, the types of lipids produced by both systems in this particular species are similar (Correa and Atehortúa, 2009). Therefore, studying Jatropha cell cultures provides additional insights about Jatropha lipid metabolism, as has been the case for cell culture models build for other plant species, for example carrot (Krook *et al.*, 1998), tomato (Rontein *et al.*, 2002), Arabidopsis (Williams *et al.*, 2008; Masakapalli *et al.*, 2010;

Cheung *et al.*, 2013; Masakapalli *et al.*, 2013) and rice (Liu *et al.*, 2013), and for other organisms, for example mammals (Lv *et al.*, 2017; van de Merbel *et al.*, 2018), where cell cultures have proved to be a valid strategy for obtaining valuable information about several aspects of metabolism.

EXPERIMENTAL PROCEDURES

Chemicals

All reagents purchased were of the highest purity available. Standards required for lipid analysis were purchased from Avanti Polar Lipids (https://avantilipids.com/), Toronto Research Chemicals (https://www.trc-canada.com/) and Sigma (https://www.sigmaaldrich.com/). For LC-MS/MS analysis of intracellular soluble metabolites, all internal standards used for quantification were prepared and handled as indicated in Arrivault *et al.* (2015). For isotope labeling studies [U-^{13}C]glucose was purchased from Cambridge Isotope Laboratories (https://www.isotope.com/) and [U-^{13}C]glycerol from Sigma, both with an isotopic purity of 99%.

Materials and equipment

The following equipment was used: a centrifuge with temperature control, orbital shaker, GC-MS column (30 m DB-35 column, Agilent Technologies, https://www.agilent.com/); LC-MS column for lipid analysis [Acquity BEH C8 column (length 100 mm, inner diameter 2.1 mm, 1.7 μm particle size; Waters, https://www.waters.com/)]; analytical balance, vacuum filtering system, convection oven, spectrophotometer, dry incubator, sonication bath, vortex, speed vacuum, Dionex ICS-3000 system; Dionex HPLC system coupled to a Finnigan TSQ quantum discovery MS-Q3 and equipped with an electrospray (ESI) interface; gas chromatograph coupled to a time-of-flight mass spectrometer (Leco Pegasus HT TOF-MS, https://leco.com/) with autosampler Gerstel multi-purpose system; ultra-performance liquid chromatography (Acquity UPLC system, Waters) coupled with a Fourier transform mass spectrometer (UPLC/FT-MS) and Orbitrap mass spectrometer (Exactive, Thermo Scientific, https://www.thermofisher.com/).

Cell suspension establishment and maintenance

Cell suspensions were established from Jatropha seeds from elite field material provided by Colombiana de Biocombustibles S.A. (http://colbio.blogspot.com/) and handled according to a previously established protocol (Correa and Atehortúa, 2012). Cell suspensions were incubated in an orbital shaker at 90 r.p.m. at 28°C in the dark.

Adaptation of cell cultures to grow with different carbon sources

The carbon source in the culture medium was supplied in the form of sucrose (gSuc). It was necessary to adapt cells to grow on glycerol (gGly) as the only carbon source. The culture medium was prepared by replacing sucrose with different combinations of glucose and glycerol. The adaptation started by subculturing cells in culture medium with a 50:50 (glucose:glycerol) composition. After 20 days of incubation a portion of 10 ml cell suspension was transferred to culture medium containing 40:60 glucose:glycerol. The same procedure was followed by varying the glucose:glycerol ratio, until cells were adapted to grow on glycerol. It was also of interest to evaluate cell growth on medium with a minimum concentration of glucose, as from preliminary experiments it was noticed that biomass content was enhanced when a small amount of glucose was included in the medium, despite this carbon source being consumed in a brief time (about 3 days) before the start of the exponential growth phase. Therefore, cells were adapted to grow on medium containing the mixture glucose:glycerol (1:9) (gMix).

Measurement of cell growth profiles

Growth profiles were measured for each growth condition. Triplicate cultures were established by transferring 75 ml of previously synchronized cell cultures to Erlenmeyer flasks containing 42 ml of the corresponding fresh medium. Cultures were incubated at 90 r.p.m. at 28°C in the dark. The time span of the sampling procedure was 15 days for gSuc and 20 days for gMix and gGly. For each replicate, a 1 ml sample was collected for biomass quantification; additional aliquots of 5 ml were taken during the exponential growth phase for biomass characterization.

The 5 ml aliquots were immediately processed by vacuum filtering. Biomass was washed twice with 10 ml portions of deionized water, collected in a tube and immediately quenched with liquid nitrogen. For biomass quantification the 1ml cell culture aliquots were centrifuged (5 min, 106 ***g***, 10°C). The supernatant was collected, transferred to new tubes, immersed in liquid nitrogen and stored at −80°C. The biomass pellet was washed twice with 2 ml portions of deionized water and centrifuged (5 min, 106 ***g***, 10°C). The supernatant was discarded and tubes with biomass were dried (12 h, 80°C). Samples were left to cool down and the weights were recorded.

Quantification of fructose consumption was done by the spectrometric modified anthrone-sulfuric method (Somani *et al.*, 1987). Quantification of total hexoses was made using the anthrone colorimetric method (Dreywood, 1946; Hansen and Møller, 1975). The glucose concentration was obtained after subtracting the fructose value of the corresponding sample from the results of total hexose quantification. Quantification of gGly was performed with an adaptation of the Nash test (Nash, 1953) and the method published by Bompelly and Skaf (2014). Measurements of inorganic ions in supernatant samples were performed by ion chromatography according to Watanabe *et al.* (2018).

Characterization of biomass composition

Substrate consumption was measured as previously described. Excretion of metabolites was not detected, as supernatants were measured through GC-MS and other compounds, apart from culture medium components, were not identified.

For the extraction and quantification of metabolic products and intermediates the biomass contained in the 5 ml aliquots was used. For extraction of lipids and internal soluble metabolites the one-step protocol from Salem *et al.* (2016) was implemented. Extraction of proteins and hydrolysis to their constitutive amino acids was done using an adapted protocol (Antoniewicz *et al.*, 2007; Masakapalli *et al.*, 2013; Salem *et al.*, 2016). For starch extraction an enzymatic digestion was performed with a mixture of amyloglusidase and α-amylase dissolved in acetate buffer (pH 4.8). After starch hydrolysis, quantification of the released glucose was done by spectrophotometry. Cell wall carbohydrates were extracted by a modified procedure from Salem *et al.* (2016) and Foster *et al.* (2010). The remaining pellet corresponded to crystalline cellulose and was pre-treated with an acid mixture of acetic acid/nitric acid/H_2O (8:1:2 v/v/v) and subsequently hydrolyzed with 72% v/v H_2SO_4. Quantification of the glucose content was performed with the previously described anthrone colorimetric method.

Internal soluble metabolites, amino acids and cell wall carbohydrates were quantified by GC-MS according to Lisec *et al.* (2006).

Chromatograms and mass spectra were evaluated using Chroma TOF 4.5 (LECO, https://www.leco.com/) and TagFinder 4.2 software.

Lipid analysis was performed by LC-MS according to procedure published by Bromke *et al*. (2015). The mass spectra were acquired using an Orbitrap mass spectrometer, and were processed with the Xcalibur and Refiner MS 7.5 (Genedata, https://www.genedata.com/) software. The output contained a list of features associated with the intensities of peaks. Features naturally containing the heavy carbon isotope (^{13}C) were removed from the data set (this step was omitted in the case of the ^{13}C-labeled samples).

Verification of the steady-state assumption

We conducted a preliminary experiment by collecting aliquots of cell suspensions during a time frame spanning the exponential growth phase (days 4–12) of gSuc. Soluble metabolites were extracted according to Arrivault *et al*. (2009) and Lunn *et al*. (2006). For quantification, internal standards were prepared as indicated in Arrivault *et al*. (2015). Anion exchange chromatography–triple quadrupole MS was performed as described in Arrivault *et al*. (2009) and Lunn *et al*. (2006). Chromatographic separation was performed with a modification of the method described by Luo *et al*. (2007). Data were normalized to dry biomass weight and reported as mmol gDW^{-1}.

Two additional sets of experiments were performed to verify the metabolic steady state. We quantified soluble metabolites of samples collected at several time points within a short interval in gSuc (day 5), gMix and gGly (day 7). The selected days corresponded to the start of the respective isotope labeling experiments. The analysis of the soluble metabolites was performed by GC-MS according to Lisec *et al*. (2006) using Chroma TOF 4.5 (Leco) and TagFinder 4.2 software for the evaluation of chromatograms and mass spectra.

The last set of experiments consisted of the quantification of lipid pools by implementing the one-step extraction protocol from Salem *et al*. (2016) with samples collected during a time lapse of the exponential growth phase of gSuc (days 5–8), gMix and gGly (days 7–9), which corresponded to the 72 h and 60 h time span where the ILEs were performed. Lipid analysis was performed by LC-MS according to the procedure published by Bromke *et al*. (2015). The mass spectra were acquired using an Orbitrap mass spectrometer and were processed with the Xcalibur and Refiner MS 7.5 (Genedata) software. From the quantification results, we determined for each growth condition if the content of metabolic intermediates varied by performing a one-way analysis of variance.

Labeling experiments and flux estimation

We implemented KFP for the experimental estimation of fluxes following the procedure described by Yuan *et al*. (2008). Kinetic flux profiling involves monitoring the dynamics of incorporation of isotope-labeled nutrient(s) into downstream products using GC/LC-MS. The essential concept of KFP is that as intracellular metabolites become labeled, there is a delay in the time-dependent profile for the unlabeled fraction between the substrate and product of an irreversible reaction. Since the time-dependent profiles of the unlabeled fraction typically follow (a combination of) exponential functions, the delay can be estimated and used to quantify the flux through a metabolic pool having access to absolute metabolite concentrations (Yuan *et al*., 2008). The labeling patterns of metabolites not only provide information about fluxes but can also be used to obtain insights about the network structure. We used the latter idea to assemble and verify parts of the model.

Labeled substrates used were [U-^{13}C]glucose for gSuc and [U-^{13}C]glycerol for gMix and gGly. The use of labeled substrates for the analysis of acyl fluxes in different plant species is thoroughly documented, including isotopically labeled gGly (Bates *et al*., 2007; Pollard *et al*., 2015a,b; Allen, 2016) and glucose (Allen, 2016).

The selected time points for the start of the ILEs were day 5 for gSuc and day 7 for gMix and gGly, for which the metabolic (quasi)steady state can be assumed and shown (see above). Jatropha cells were prepared in advance by selecting cell cultures in the exponential growth phase having viability values of at least 90%. To perform the ILEs, cells were filtered and immediately transferred to medium with the corresponding labeled substrates, conducting this step as fast as possible to avoid disturbances in metabolism. Sampling was carried out at different time points for a duration of 72 h. Cell samples were fast filtered and metabolism was quenched with liquid nitrogen. Samples were stored at −80°C. For the extraction and quantification of metabolites, the procedures previously described for lipid extraction were implemented. The correction for natural abundance of isotopes of raw data was performed with IsoCor software, version 1.0 (Millard *et al*., 2012). After correction for natural abundance of isotopes, the mathematical treatment of the data was done as described in Yuan *et al*. (2008). The calculations were performed for all the metabolites for which the necessary data were available (Table S1) (Figure 2).

Metabolic network reconstruction

The model consisted of 800 reactions, 647 metabolites and 8 compartments. Here we would like to emphasize that even though the genome from Jatropha was sequenced and that there is also the possibility to apply automated tools to perform a bottom-up reconstruction, it must be noted that we were interested in lipid metabolism for which there is no complete annotation and thus these approaches will not provide optimal results. We also checked other plant metabolic models of small (Schwender *et al*., 2004, 2006; Junker *et al*., 2007; Alonso *et al*., 2007a,b; Williams *et al*., 2008; Allen *et al*., 2009; Lonien and Schwender, 2009; Alonso *et al*., 2010, 2011; Kruger *et al*., 2012; Allen and Young, 2013; Masakapalli *et al*., 2013; Colombié *et al*., 2015; Schwender *et al*., 2015; Rossi *et al*., 2017; Cocuron *et al*., 2019) and medium size (Grafahrend-Belau *et al*., 2009; Pilalis *et al*., 2011; Hay and Schwender, 2011a,b; Schwender and Hay, 2012; Grafahrend-Belau *et al*., 2013; Arnold and Nikoloski, 2014), besides the available genome-scale models (GEMs) (Poolman *et al*., 2009; Radrich *et al*., 2010; Dal'Molin *et al*., 2010; Saha *et al*., 2011; Mintz-Oron *et al*., 2012; Poolman *et al*., 2013; Monaco *et al*., 2013; Simons *et al*., 2014; Seaver *et al*., 2015; Lakshmanan *et al*., 2015; Yuan *et al*., 2016; Bogart and Myers, 2016; Chatterjee *et al*., 2017; Botero *et al*., 2018; Pfau *et al*., 2018; Shaw and Cheung, 2018; Moreira *et al*., 2019), and found that most of the metabolic reconstructions of small and medium size have low levels of detail of the lipid network, since the lipid-related reactions are lumped. The exception is the metabolic reconstruction for rapeseed (Hay and Schwender, 2011a,b), with a total of 572 reactions of which 187 are lipid-related. After reviewing the GEM structure, we found that FA synthesis and lipid degradation reactions were detailed; however, the reactions of structural lipid synthesis (e.g. galactolipids and sulfolipids) and phospholipid formation were lumped to a greater or lesser extent. Further, we found that in most of the examined GEMs, the ER compartment was not included, although important reactions of glycerolipid formation, acyl editing and phospholipid

synthesis, among others, take place in this compartment. We also found that storage lipid formation (i.e. TAG) was represented by a single lumped reaction. Exceptions are the rice GEM (iOS2164) (Lakshmanan *et al.*, 2015) and the evidence-based maize GEM (Seaver *et al.*, 2015) models. For these reasons, we decided not to make use of these automated tools and to perform a bottom-up reconstruction.

Diverse bibliomic data were examined to allow up-to-date accurate reconstruction for storage and structural lipid biosynthetic pathways. The topology of the lipid biosynthesis network was refined with the aid of different resources such as the Jatropha Genome Database (http://www.kazusa.or.jp/jatropha/), KEGG, the enzyme repository BRENDA and the universal protein database (UniProt). The Aralipid website (http://aralip.plantbiology.msu.edu/pathways/pathways) (Li-Beisson *et al.*, 2013) was also consulted to compare the structure of the lipid network. The findings from the ILEs were also used for refinement purposes.

Some reactions of the lipid network that were adjacent without known branching points were combined into lumped reactions, for example the set of reactions catalyzed by the FAS complex leading to C16:0- and C18:0-acyl species; the reaction catalyzed by lipases to hydrolyze TAG; the catabolic process of β-oxidation to break down FA molecules into acyl-CoA units; the sequential reactions catalyzed by LPAAT and PAP enzymes in the Kennedy pathway to produce DAG; and the reactions catalyzed by phospholipase A2 and the long-chain acyl-CoA synthetase that cleave the FA attached in the *sn*-2 position of PC, following their activation to acyl-CoA, respectively, that takes place during the acyl editing process.

The inclusion of extracellular transport reactions, and the allocation of intracellular transport reactions, was based on an extensive literature search to have confidence about location, stoichiometry and transport mechanisms. Additional transporters were added when necessary, to ensure production of biomass. Glycerol assimilation and metabolism was included, as this was the carbon source in two of the growth conditions evaluated, supported by an analogous mechanism reported for *R. communis* (Eastmond, 2004). Reactions for the synthesis of cell wall components appear in the Golgi apparatus, based on literature from different sources (Kleczkowski *et al.*, 2010; Li *et al.*, 2011). Glycolysis and the PPP reactions were included in the cytosol and plastids. These pathways were found duplicated in both compartments in cells from seed endosperm of *R. communis* (Ireland and Dennis, 1981; Miernyk and Dennis, 1982, 1992). There is also evidence of the duplication of these pathways in other species [e.g. carrot (Krook *et al.*, 1998), soybean (Sriram *et al.*, 2004), corn (Alonso *et al.*, 2010), sunflower (Alonso *et al.*, 2007a) and Arabidopsis (Lonien and Schwender, 2009)]. Reactions were additionally considered to account for the energy expenditure in protein polymerization and processing (Woese *et al.*, 2000; Mathews *et al.*, 2002). The glyoxysome compartment was included, as in cells from oleaginous tissues (e.g. seed endosperm) this is the subcellular location where the metabolism of storage lipids occurs (Quettier and Eastmond, 2009; Barros *et al.*, 2010). In mitochondria, the TCA cycle, oxidative phosphorylation, proline and glutamine metabolism were included.

A condition-specific biomass reaction was constructed, using the experimental data obtained from the biomass characterization procedure.

The growth associated maintenance (GAM) and NGAM parameters can be derived from chemostat culture data, as has been done for bacteria and yeast cells (Varma and Palsson, 1994). In addition, they can be used along with assumptions regarding the proportional change of the values of GAM and NGAM as done for microorganisms with few experimental data available (Borodina *et al.*, 2005; Feist *et al.*, 2006; Lee *et al.*, 2008). However, given the technical difficulties involved in the implementation of this methodology, its usage with other organisms, such as plants, is not straightforward. Further, measurements of the cost of maintenance generally do not provide information about the partitioning between ATP and NADPH demands. Therefore, to estimate the NGAM costs we made a literature search to gain an overview about how this parameter was estimated and incorporated in plant models (Poolman *et al.*, 2009; Grafahrend-Belau *et al.*, 2009; Dal'Molin *et al.*, 2010; Radrich *et al.*, 2010; Hay and Schwender, 2011b; Pilalis *et al.*, 2011; Saha *et al.*, 2011; Mintz-Oron *et al.*, 2012; Cheung *et al.*, 2013; Grafahrend-Belau *et al.*, 2013; Monaco *et al.*, 2013; Poolman *et al.*, 2013; Arnold and Nikoloski, 2014; Simons *et al.*, 2014; Lakshmanan *et al.*, 2015; Seaver *et al.*, 2015; Bogart and Myers, 2016; Yuan *et al.*, 2016; Chatterjee *et al.*, 2017; Botero *et al.*, 2018; Pfau *et al.*, 2018; Shaw and Cheung, 2018; Moreira *et al.*, 2019). In only three of the reviewed models (Poolman *et al.*, 2009, 2013; Cheung *et al.*, 2013) the respective calculations of the maintenance costs were made using different approaches and experimental data for the respective biological systems, and in turn the reported NGAM costs were used in other published studies (Hay and Schwender, 2011b; Yuan *et al.*, 2016; Chatterjee *et al.*, 2017; Shaw and Cheung, 2018; Moreira *et al.*, 2019). There were other models whose maintenance costs were entirely taken from the literature (Grafahrend-Belau *et al.*, 2009; Pfau *et al.*, 2018). After comparing the respective publications, we analyzed several scenarios to select the most convenient method for integrating the maintenance costs in the model considering the limitations of our system set-up and the experimental data available.

i We considered the use of biomass, transport costs and KFP-estimated fluxes, without the NGAM costs. However, this resulted in a relatively poor prediction of the fluxes through central metabolism, especially for the PPP pathway, whose fluxes can be substantially underestimated: the oxidative branch of the plastidial and cytosolic PPP appeared totally or partially inactive or carried negligible fluxes when predicting fluxes at optimum condition-specific growth (setting condition-specific biomass synthesis as an objective function) or when performing total flux minimization, while there is evidence of its operation in heterotrophic plant cell cultures (Williams *et al.*, 2010) as well as in cells from seed endosperm of *R. communis* (Ireland and Dennis, 1981; Miernyk and Dennis, 1982, 1992) and other plant species [e.g. carrot (Krook *et al.*, 1998), soybean (Sriram *et al.*, 2004), corn (Alonso *et al.*, 2010), sunflower (Alonso, Goffman, *et al.*, 2007) and Arabidopsis (Lonien and Schwender, 2009)]. In addition, the predicted fluxes for substrate consumption did not match the experimental values, as was also observed in the analysis made by Cheung *et al.* (2013).

ii Another possibility was to assign values iteratively to a generic ATPase step until the carbon consumption rate matched the experimental values, as done in Poolman *et al.* (2009), Williams *et al.* (2010) and Hay and Schwender (2011b). While it is possible in this way to match the predicted to the measured substrate consumption values it is also necessary to keep in mind the inconvenience of expressing the maintenance costs solely in terms of ATP, since maintenance costs can vary widely from one tissue and/or environmental growth condition to another. Therefore, the accuracy of the predicted maintenance ATP cost will be dependent on how close the flux balance solutions are to the actual metabolic flux state (Sweetlove and George Ratcliffe, 2011; Colombié *et al.*, 2015).

This has led to an overestimation of some pathways in their contribution to cell maintenance (i.e. the TCA cycle, glycolysis), while other pathways are underestimated [i.e. the oxidative pentose phosphate pathway (OPPP)], although their role *in vivo* is well documented (Williams *et al.*, 2010). Therefore, the evidence suggests that in plants it is advisable to divide the maintenance costs between ATP and NADPH, and it is also necessary to consider that these costs may vary under different conditions (Sweetlove *et al.*, 2013).

iii Another possibility for including both the generic ATPase and NADPH steps is given by the Pareto approach to estimating the NGAM (ATP and NADPH) costs, as explained in Cheung *et al.* (2013). This approach was used to explore the ATP–NADPH trade-off operating in the generation of ATP and NADPH, as the pathways that produce them compete for the same hexose phosphate precursors. In this approach, the model is constrained with the experimental values of glucose consumption and the biomass production rates, and the fluxes through the generic ATPase and NADPH oxidase reactions are maximized. As a result a set of Pareto optimal solutions are identified that correspond to different flux distributions in the metabolic network, whose ATP and NADPH maintenance costs result in a match to the experimentally measured rates of carbon consumption. Here it is important to highlight that in the Pareto optimal solution the ATP:NADPH ratios are different, which means in turn a variation in the flux ratios between the oxidative steps of the OPPP (generating NADPH) and glycolysis (leading to ATP generation) as the maintenance demand switches from NADPH to ATP. Given that a set of solutions is obtained, it might be problematic to select one Pareto optimal solution over the others without any previous knowledge about the flux ratios for key branch points where metabolic intermediates are diverted either to ATP or NADPH generation.

iv An option to address the issue of not having specific information available for Jatropha cells related to the OPPP:glycolysis ratio might make use of the flux ratio measured by Cheung *et al.* (2013), as this work was performed for Arabidopsis cell cultures fed with glucose as the carbon source. However, it has been observed that the relative contribution of NADPH and ATP to the maintenance cost strongly depends on the conditions imposed on the cell culture, as was the case for Arabidopsis cells. In Arabidopsis the predicted value for the NADPH:ATP maintenance ratio was 0.35 for control conditions, but this switched under stress conditions to 0.84 in hyper-osmotic conditions and to 0.19 at elevated temperature. In the experiments made with Jatropha cells, the composition of the medium is relatively similar in one of the conditions; however, the carbon source is different for the remaining growth conditions. Besides, the growth temperature of Jatropha cells is different from that of Arabidopsis cells, thus it might be expected that NGAM requirements, as well as the ATP:NADPH ratios, could differ among the cell culture systems, which raise doubts about the convenience of using the experimental values measured for cell cultures of other plant species grown under different environmental conditions.

v The last scenario evaluated was to make use of the data available (i.e. measurements from biomass composition, substrate consumption and growth rates) to implement the procedure explained next and that was based on the approach used by Cheung *et al.* (2013): (a) the initial step was the calculation of the transport costs by using the experimental data for substrate consumption; (b) next, the GAM costs (ATP, NADH and NADPH) were estimated by using the experimental data of biomass composition. First, the main biomass components were identified as well as their respective metabolite precursors; the ATP, NADH and NADPH stoichiometry was then determined for each of the biomass components. The model was afterwards constrained using the measured rates of substrate consumption, the condition-specific biomass reaction and the measured rate of biomass production. This was followed by total flux minimization and the obtained fluxes were used to estimate the GAM (ATP, NADH and NADPH). (c) In the last step, the NGAM (ATP and NADPH) cost was estimated by first estimating the total ATP and NADPH produced by the metabolic pathways of central metabolism using the flux distribution obtained in the step (b) from total flux minimization. Then, the values obtained for GAM (ATP, NADH and NADPH) were subtracted from the respective total values calculated for ATP, NADH and NADPH, so the residual values were assumed to correspond to the NGAM (Table S12). To account for these NGAM costs, generic ATP and NADPH hydrolysis steps were added to the model (Cheung *et al.*, 2013). The energy expenditure for transportation, in the form of ATP was accounted for by including a plasma membrane ATPase step constrained with the calculated values.

Model constraints and implementation

With the constructed mass- and charge-balanced model, a set of constraints were defined for each growth condition and subsequently included in the model (Table S2): (i) the extracellular fluxes, (ii) the NGAM (i.e. ATP and NADPH) costs calculated for each growth condition, (iii) the energy expenditure in transport processes, (iv) the KFP-estimated fluxes, and (v) the condition-specific biomass reaction. For network verification, evaluation and validation, the COBRA Toolbox was used (Thiele and Palsson, 2010; Schellenberger *et al.*, 2011). Several functions of the COBRA Toolbox were used to check the charge and mass balance of the reactions included in the model and for detecting missing metabolic functions (gaps), metabolic dead-ends, blocked reactions and stoichiometrically balanced cycles. When any of the late issues were detected, a detailed revision was made and the corresponding corrective measures were applied as detailed in Thiele and Palsson (2010). Demand reactions were added for several cofactors (i.e. CoA, NAD, NADP) because they were detected to participate in blocked reactions even when the respective metabolites were well connected in the metabolic network and were not identified as gap metabolites. The reason for this discrepancy was due to the 'coenzyme pseudo-gap problem', occurring when the biosynthetic pathway for the *de novo* synthesis of a particular molecule is included in the reconstruction (as is our case), but there are no fluxes draining or degrading the said molecule produced by this pathway. Ponce-de-León *et al.* (2013) described that these metabolites may be involved in conserved moieties, and in such cases they will be consumed and regenerated in a cyclic manner. As a consequence they could not be detected as gap metabolites because they will participate in at least two active reactions. However, if the biosynthetic pathway for a coenzyme is included in a metabolic model, the net production of a coenzyme will not occur under steady-state conditions unless some flux consumes it (Ponce-de-León *et al.*, 2013). Hence, the reactions involved in the biosynthesis pathway may become blocked, as in our case. A common approach to solve this situation is to include the coenzyme-like metabolite into the biomass equation; however, as we do not have direct experimental measurements of these coenzyme concentrations in the biomass, the alternative is to introduce an exchange flux that can

drain the metabolite out of the system, which was done by introducing the demand reactions.

The rate of growth was evaluated and compared with the experimentally measured rates. The model in SBML format can be found in Data S1.

Incorporation of labeling data as experimental constraints

Flux variability analysis was performed for each growth condition, with and without including the KFP-estimated fluxes, as constraints. The *fluxVariability()* function of the COBRA Toolbox was used, with three sets of constraints, each one containing the condition-specific experimental information, in addition to the KFP-estimated fluxes. The resulting flux intervals were compared for the three growth conditions and the fluxes for which a decrease in magnitude was observed were selected for calculation of the total percentage of reduction of all the flux values analyzed.

Implementation of FSEOF

The flux distributions were calculated through constrained-based analysis using the COBRA Toolbox software installed on a personal computer (2.40 GHz Intel Core CPU and Windows 10 Pro platform). The FSEOF procedure was implemented following the procedure described in Choi *et al.* (2010) with some modifications.

i First, the reference fluxes ($vj^{initial}$) were calculated by maximizing the flux through the condition-specific biomass reaction. For this calculation, the model was constrained with the experimentally determined biomass composition, the remaining environmental constraints (substrate consumption rates) including the KFP-estimated fluxes and the calculated NGAM costs. The optimum condition-specific growth was calculated as indicated: maximize $v_{biomass}$ subject to $\sum_{(j=1)}^{N} S_{ij} v_j = 0$ and $v_j^{\alpha} \le v_j \le v_j^{\beta}$, where $v_{biomass}$ represents the biomass formation rate, S_{ij} is the stoichiometric coefficient of metabolite *i* in the *j*th reaction, v_j is the flux of the jth reaction, and v_j^{α} and v_j^{β} are the lower and upper bounds of the flux of the *j*th reaction, respectively. The optimum growth rate was subsequently used to constrain the lower bound of the biomass reaction and this was followed by minimization of the total flux, commonly applied to reduce the set of possible solutions (Holzhütter, 2004; Sweetlove and George Ratcliffe, 2011; Colombié *et al.*, 2015) (implemented using the function [MinimizedFlux modelIrrev]= minimizeModelFlux(model) of the COBRA Toolbox) that can be expressed as: minimize $\| v_0 \|$ subject to $\sum_{(j=1)}^{N} S_{ij} v_j = b$ and $v_j^{\alpha} \le v_j \le v_j^{\beta}$, and $v_{biomass}^{\alpha} = v_{biomass}^{opt}$, where *b* is the exchange flux vector, $v_{biomass}^{\alpha}$ is the lower bound of the biomass reaction and $v_{biomass}^{opt}$ is the optimum condition-specific growth rate.

ii Then, the theoretical maximum product (i.e. C18:1 and total TAGs, produced by the SACPD and LBF reactions, respectively) formation rates were calculated by FBA. This was done by setting the objective function as maximizing the product formation flux during the constraint-based flux analysis, which can be formulated as follows: maximize $v_{product}$ subject to $\sum_{(j=1)}^{N} S_{ij} v_j = 0$ and $v_j^{\alpha} \le v_j \le v_j^{\beta}$, where $v_{product}$, represents the accumulation rate of either C18:1 or TAG. For the scenario where the goal was to maximize the accumulation of both target metabolites, a Pareto optimality analysis was performed to obtain the theoretical maximum for two objective functions by simultaneously optimizing the two reactions leading to the formation of the mentioned products, by implementing the COBRA Toolbox function [ParetoFrontier] = compute ParetoOptimality(A,'Rxn1','Rxn2'). Then, the Pareto frontier was examined to select the theoretical maximum for both reactions and the respective values were used to constrain the lower bounds of SACPD and LBF.

iii Finally, FSEOF was carried out during the constraint-based flux analysis under the objective function of maximizing cell growth while the target metabolite production rate was set (enforced) to a value similar to the respective theoretical maximum value. The process of enforcing the target metabolite rates was done iteratively by initially constraining the rates to the respective theoretical maximum values and, when the biomass formation rate became zero, the rates were gradually reduced until obtaining a feasible flux distribution.

To obtain the flux distribution after enforcing the target reactions the following calculations were made: minimize $\| v_0 \|$ subject to $v_{product}^{enforced} = v_{product}^{max} - \left(v_{product}^{max} \times n \right)$ (where $n \le 0.05$), subject to $\sum_{(j=1)}^{N} S_{ij} v_j = b$ and $v_j^{\alpha} \le v_j \le v_j^{\beta}$, and $v_{biomass}^{\alpha} = v_{biomass}^{opt}$ where $v_{product}^{enforced}$ is the additional constraint provided during the constraint-based flux analysis to enforce the formation of the target metabolites, which starts with the theoretical maximum value $v_{product}^{max}$ and, if the biomass formation rate became zero, the product of the multiplication $v_{product}^{max} \times n$ is subtracted from $v_{product}^{max}$, in an iterative process until obtaining a feasible flux distribution.

We examined a fourth scenario where in addition to the maximization of cell growth while the production rates of the target metabolites were enforced, we made the pathway of storage lipid degradation inoperative. In plants and yeast, the major pathway for metabolic breakdown of FAs is β-oxidation occurring in peroxisomes (Graham, 2008; Theodoulou and Eastmond, 2012) or in the glyoxysome as is the case of cells from seed endosperm (Quettier and Eastmond, 2009; Barros *et al.*, 2010). Before β-oxidation can take place, storage lipids must be hydrolyzed, and the released FAs must be transported to the peroxisome or glyoxysome. For the hydrolysis of TAGs there are several enzymes identified with lipase activity (i.e. SDP1, SDP1L and ATGLL) (Fan *et al.*, 2014), and for mobilization of FAs to this organelle a transporter (i.e. PXA1) was identified (De Marcos Lousa *et al.*, 2013). In this scenario, we knocked out these two key processes, which has already been evaluated as a successful integral engineering strategy to boost TAG accumulation in plant seeds and leaves (Kelly *et al.*, 2013; Fan *et al.*, 2014; van Erp *et al.*, 2014; Vanhercke *et al.*, 2017).

Subsequently, we selected the overexpression targets by identifying the reactions whose fluxes increased upon the application of the enforced objective flux without changing the direction of the reaction. This can be formulated as: select v_j that satisfies $|v_j^{max}| > |v_j^{initial}|$ and $v_j^{max} \times v_j^{min} \ge 0$ where the v_j^{max} and v_j^{min} are the maximum and minimum fluxes of the *j*th reaction calculated during the FSEOF implementation by performing FVA.

Software availability

The scripts used for the modeling procedures and the data analysis are available online at GitHub: https://github.com/marce2336/JcLipidWorflow.

ACKNOWLEDGEMENTS

Thanks to the Biotechnology Laboratory-Universidad de Antioquia and the Max Planck Institute of Molecular Plant Physiology for the use of their infrastructure. Thanks to Änne Michaelis, Gudrun Wolter, André Scheffel, Arun Sampathkumar, Rainer Höfgen, Franziska Brückner, Stephanie Arrivault, Manuela Guenther, Patrick Giavalisco, Laise Rosado, Elmien Heyneke, José Vallarino, Fayezeh Arabi, Karin Köhl, Regina Wendenburg and Ina Krahnert for their assistance during different parts of the experimental work. We are grateful to Carlos Palacio (Colombiana de Biocombustibles) for supplying the plant material, to Néstor Giraldo and Luis Velasquez

for their assistance with some aspects of the experimental work and to Michael Scheunemann for his help with some technical issues in the modeling procedure. The work was financially supported by Fondo Nacional de Financiamiento para la Ciencia, la Tecnología y la Innovación Francisco José de Caldas-Colciencias (grant no. 617/2013) and the DAAD (grant no. 57214225).

AUTHOR CONTRIBUTIONS

RRE, LA, ZN, ARF and SMC designed the research. SMC performed the experiments. YB assisted with the lipidomic analysis. SA contributed to the chromatographic analysis and interpretation of data. ZN, RRE and LA assisted with data analysis and manuscript preparation. ZN and SMC constructed and validated the metabolic model and made the modeling and computational analysis. ZN, ARF and SMC wrote the article. All authors contributed to the last version of the manuscript.

CONFLICT OF INTEREST

The authors declare that the research was conducted in the absence of any commercial or financial relationships that could be construed as a potential conflict of interest.

SUPPORTING INFORMATION

Additional Supporting Information may be found in the online version of this article.

Table S1. Labeled lipid species identified.

Table S2. Condition-specific constraints.

Table S3. Verification metabolic steady state.

Table S4. Biomass components quantification.

Table S5. Reducing power calculations.

Table S6. Kinetic flux profiling-estimated fluxes.

Table S7. Correlation coefficient KFP-estimated fluxes.

Table S8. Pairwise comparison.

Table S9. Flux bound reduction.

Table S10. Flux scanning based on enforced objective flux.

Table S11. Flux coupling analysis.

Table S12. GAM and NGAM calculations.

Data S1. *Jatropha curcas* model.

REFERENCES

Abbadi, A. and Leckband, G. (2011) Rapeseed breeding for oil content, quality, and sustainability. *Eur. J. Lipid Sci. Technol.* **113**, 1198–1206.

Akintayo, E.T. (2004) Characteristics and composition of *Parkia biglobbossa* and *Jatropha curcas* oils and cakes. *Bioresour. Technol.* **92**, 307–310.

Allen, D.K. (2016) Assessing compartmentalized flux in lipid metabolism with isotopes. *Biochim. Biophys. Acta Mol. Cell Biol. Lipids*, **1861**, 1226–1242.

Allen, D.K., Bates, P.D. and Tjellström, H. (2015) Tracking the metabolic pulse of plant lipid production with isotopic labeling and flux analyses: past, present and future. *Prog. Lipid Res.* **58**, 97–120.

Allen, D.K., Ohlrogge, J.B. and Shachar-Hill, Y. (2009) The role of light in soybean seed filling metabolism. *Plant J.* **58**, 220–234.

Allen, D.K. and Young, J.D. (2013) Carbon and nitrogen provisions alter the metabolic flux in developing soybean embryos. *Plant Physiol.* **161**, 1458–1475.

Almaas, E., Kovács, B., Vicsek, T., Oltvai, Z.N. and Barabási, A.L. (2004) Global organization of metabolic fluxes in the bacterium *Escherichia coli*. *Nature*, **427**, 839–843.

Alonso, A.P., Dale, V.L. and Shachar-Hill, Y. (2010) Understanding fatty acid synthesis in developing maize embryos using metabolic flux analysis. *Metab. Eng.* **12**, 488–497.

Alonso, A.P., Goffman, F.D., Ohlrogge, J.B. and Shachar-Hill, Y. (2007a) Carbon conversion efficiency and central metabolic fluxes in developing sunflower (*Helianthus annuus* L.) embryos. *Plant J.* **52**, 296–308.

Alonso, A.P., Raymond, P., Rolin, D. and Dieuaide-Noubhani, M. (2007b) Substrate cycles in the central metabolism of maize root tips under hypoxia. *Phytochemistry*, **68**, 2222–2231.

Alonso, A.P., Val, D.L. and Shachar-Hill, Y. (2011) Central metabolic fluxes in the endosperm of developing maize seeds and their implications for metabolic engineering. *Metab. Eng.* **13**, 96–107.

Antoniewicz, M.R., Kraynie, D.F., Laffend, L.A., González-Lergier, J., Kelleher, J.K. and Stephanopoulos, G. (2007) Metabolic flux analysis in a nonstationary system: fed-batch fermentation of a high yielding strain of *E. coli* producing 1,3-propanediol. *Metab. Eng.* **9**, 277–292.

Arnold, A. and Nikoloski, Z. (2014) Bottom-up metabolic reconstruction of Arabidopsis and its application to determining the metabolic costs of enzyme production. *Plant Physiol.* **165**, 1380–1391.

Arrivault, S., Guenther, M., Fry, S.C., Fuenfgeld, M.M.F.F., Veyel, D., Mettler-Altmann, T., Stitt, M. and Lunn, J.E. (2015) Synthesis and use of stable-isotope-labeled internal standards for quantification of phosphorylated metabolites by LC-MS/MS. *Anal. Chem.* **87**, 6896–6904.

Arrivault, S., Guenther, M., Ivakov, A., Feil, R., Vosloh, D., Dongen, J.T.V., Sulpice, R. and Stitt, M. (2009) Use of reverse-phase liquid chromatography, linked to tandem mass spectrometry, to profile the Calvin cycle and other metabolic intermediates in Arabidopsis rosettes at different carbon dioxide concentrations. *Plant J.* **59**, 824–839.

Bansal, S., Kim, H.J., Na, G., Hamilton, M.E., Cahoon, E.B., Lu, C. and Durrett, T.P. (2018) Towards the synthetic design of camelina oil enriched in tailored acetyl-triacylglycerols with medium-chain fatty acids. *J. Exp. Bot.* **69**, 4395–4402.

Bao, X., Focke, M., Pollard, M. and Ohlrogge, J. (2000) Understanding *in vivo* carbon precursor supply for fatty acid synthesis in leaf tissue. *Plant J.* **22**, 39–50.

Barros, M., Fleuri, L.F. and Macedo, G.A. (2010) Seed lipases: sources, applications and properties—a review. *Braz. J. Chem. Eng.* **27**, 15–29.

Bates, P.D. (2016) Understanding the control of acyl flux through the lipid metabolic network of plant oil biosynthesis. *Biochim. Biophys. Acta Mol. Cell Biol. Lipids*, **1861**, 1214–1225.

Bates, P.D., Durrett, T.P., Ohlrogge, J.B. and Pollard, M. (2009) Analysis of acyl fluxes through multiple pathways of triacylglycerol synthesis in developing soybean embryos. *Plant Physiol.* **150**, 55–72.

Bates, P.D., Ohlrogge, J.B. and Pollard, M. (2007) Incorporation of newly synthesized fatty acids into cytosolic glycerolipids in pea leaves occurs via acyl editing. *J. Biol. Chem.* **282**, 31206–31216.

Bates, P.D., Stymne, S. and Ohlrogge, J. (2013) Biochemical pathways in seed oil synthesis. *Curr. Opin. Plant Biol.* **16**, 358–364.

Baud, S. and Lepiniec, L. (2010) Physiological and developmental regulation of seed oil production. *Prog. Lipid Res.* **49**, 235–249.

Beevers, H. (1980) The role of glyoxylate cycle. In *Biochemistry of Plants*. (Stumpf, P. and Conn, E., eds). New York: Academic Press, pp. 117–130.

Bogart, E. and Myers, C.R. (2016) Multiscale metabolic modeling of C4 plants: connecting nonlinear genome-scale models to leaf-scale metabolism in developing maize leaves. *PLoS One*, **11**(3), e0151722.

Bompelly, R. and Skaf, D.W. (2014) Optimization of a colorimetric test method for quantifying glycerol in aqueous solution. *J. Am. Oil Chem. Soc.* **91**, 1605–1610.

Borisjuk, L., Neuberger, T., Schwender, J. *et al.* (2013) Seed architecture shapes embryo metabolism in oilseed rape. *Plant Cell*, **25**, 1625–1640.

Borodina, I., Krabben, P. and Nielsen, J. (2005) Genome-scale analysis of *Streptomyces coelicolor* A3(2) metabolism. *Genome Res.* **15**, 820–829.

Botero, K., Restrepo, S. and Pinzón, A. (2018) A genome-scale metabolic model of potato late blight suggests a photosynthesis suppression mechanism. *BMC Genom.*, **19**, 31–44.

Bromke, M.A., Hochmuth, A., Tohge, T., Fernie, A.R., Giavalisco, P., Burgos, A., Willmitzer, L. and Brotman, Y. (2015) Liquid chromatography high-resolution mass spectrometry for fatty acid profiling. *Plant J.* **81**, 529–536.

Chatterjee, A., Huma, B., Shaw, R. and Kundu, S. (2017) Reconstruction of *Oryza sativa* indica genome scale metabolic model and its responses to

varying RuBisCO activity, light intensity, and enzymatic cost conditions. *Front. Plant Sci.* **8**, 2060.

Chen, M., Mooney, B.P., Hajduch, M., Joshi, T., Zhou, M., Xu, D. and Thelen, J.J. (2009) System analysis of an Arabidopsis mutant altered in de novo fatty acid synthesis reveals diverse changes in seed composition and metabolism. *Plant Physiol.* **150**, 27–41.

Cheung, C.Y.M., Williams, T.C.R., Poolman, M.G., Fell, D.A., Ratcliffe, R.G. and Sweetlove, L.J. (2013) A method for accounting for maintenance costs in flux balance analysis improves the prediction of plant cell metabolic phenotypes under stress conditions. *Plant J.* **75**, 1050–1061.

Choi, H.S., Lee, S.Y., Kim, T.Y. and Woo, H.M. (2010) *In silico* identification of gene amplification targets for improvement of lycopene production. *Appl. Environ. Microbiol.* **76**, 3097–3105.

Cocuron, J.C., Koubaa, M., Kimmelfield, R., Ross, Z. and Alonso, A.P. (2019) A combined metabolomics and fluxomics analysis identifies steps limiting oil synthesis in maize embryos. *Plant Physiol.* **181**, 961–975.

Colombié, S., Nazaret, C., Bénard, C. *et al.* (2015) Modelling central metabolic fluxes by constraint-based optimization reveals metabolic reprogramming of developing *Solanum lycopersicum* (tomato) fruit. *Plant J.* **81**, 24–39.

Correa, S. and Atehortúa, L. (2009) *In vitro* biomass and oil production of *Jatropha curcas*. In *Proceedings of the 17th European Biomass Conference and Exhibition*. Hamburg.

Correa, S.M. and Atehortúa, L. (2012) Lipid profile of *in vitro* oil produced through cell culture of *Jatropha curcas*. *J. AOAC Int.* **95**, 1161–1169.

Costa, G.G.L., Cardoso, K.C., Bem, L.E.V.D. *et al.* (2010) Transcriptome analysis of the oil-rich seed of the bioenergy crop *Jatropha curcas* L. *BMC Genom.*, **11**, 462.

Dahlqvist, A., Ståhl, U., Lenman, M., Banas, A., Lee, M., Sandager, L., Ronne, H. and Stymne, S. (2000) Phospholipid:diacylglycerol acyltransferase: an enzyme that catalyzes the acyl-CoA-independent formation of triacylglycerol in yeast and plants. *Proc. Natl Acad. Sci. USA*, **97**, 6487–6492.

de Oliveira Dal'Molin, C.G., Quek, L.E., Palfreyman, R.W., Brumbley, S.M. and Nielsen, L.K. (2010) AraGEM, a genome-scale reconstruction of the primary metabolic network in Arabidopsis. *Plant Physiol.* **152**, 579–589.

Dörmann, P., Voelker, T.A. and Ohlrogge, J.B. (2000) Accumulation of palmitate in Arabidopsis mediated by the acyl-acyl carrier protein thioesterase FATB1. *Plant Physiol.* **123**, 637–643.

Dreywood, R. (1946) Qualitative test for carbohydrate material. *Ind. Eng. Chem. Anal. Ed.* **18**, 499.

Drincovich, M.F., Casati, P. and Andreo, C.S. (2001) NADP-malic enzyme from plants: a ubiquitous enzyme involved in different metabolic pathways. *FEBS Lett.* **490**, 1–6.

Durrett, T.P., McClosky, D.D., Tumaney, A.W., Elzinga, D.A., Ohlrogge, J. and Pollard, M. (2010) A distinct DGAT with sn-3 acetyltransferase activity that synthesizes unusual, reduced-viscosity oils in *Euonymus* and transgenic seeds. *Proc. Natl Acad. Sci. USA*, **107**, 9464–9469.

Eastmond, P.J. (2004) Glycerol-insensitive Arabidopsis mutants: gli1 seedlings lack glycerol kinase, accumulate glycerol and are more resistant to abiotic stress. *Plant J.* **37**, 617–625.

van Erp, H., Bates, P.D., Burgal, J., Shockey, J. and Browse, J. (2011) Castor phospholipid: diacylglycerol acyltransferase facilitates efficient metabolism of hydroxy fatty acids in transgenic Arabidopsis. *Plant Physiol.* **155**, 683–693.

van Erp, H., Kelly, A.A., Menard, G. and Eastmond, P.J. (2014) Multigene engineering of triacylglycerol metabolism boosts seed oil content in Arabidopsis. *Plant Physiol.* **165**, 30–36.

van Erp, H., Shockey, J., Zhang, M., Adhikari, N.D. and Browse, J. (2015) Reducing isozyme competition increases target fatty acid accumulation in seed triacylglycerols of transgenic Arabidopsis. *Plant Physiol.* **168**, 36–46.

Fan, J., Yan, C., Roston, R., Shanklin, J. and Xu, C. (2014) Arabidopsis lipins, PDAT1 ACYLTRANSFERASE, and SDP1 triacylglycerol lipase synergistically direct fatty acids toward β-oxidation, thereby maintaining membrane lipid homeostasis. *Plant Cell*, **26**, 4119–4134.

Feist, A.M., Scholten, J.C.M., Palsson, B., Brockman, F.J. and Ideker, T. (2006) Modeling methanogenesis with a genome-scale metabolic reconstruction of *Methanosarcina barkeri*. *Mol. Syst. Biol.* **2**, 2006.0004. https://doi.org/10.1038/msb4100046

Fonseca, L.R., Silva Sá, J.L. and Lima-Neto, B.S. (2016) Plant oil-based polyester. In *Bio-Based Plant Oil Polymers and Composites* (Madbouly, S.A., Chaoqun, Z. and Michael, R.K., eds). Norwich, NY: William Andrew, pp. 73–86.

Foster, C.E., Martin, T.M. and Pauly, M. (2010) Comprehensive compositional analysis of plant cell walls (lignocellulosic biomass) part II: carbohydrates. *J. Vis. Exp.*, 1837. https://doi.org/10.3791/1837

Ghosh, A., Ando, D., Gin, J. *et al.* (2016) ^{13}C metabolic flux analysis for systematic metabolic engineering of *S. cerevisiae* for overproduction of fatty acids. *Front. Bioeng. Biotechnol.* **4**, 76.

Grafahrend-Belau, E., Junker, A., Eschenröder, A., Müller, J., Schreiber, F. and Junker, B.H. (2013) Multiscale metabolic modeling: dynamic flux balance analysis on a whole-plant scale. *Plant Physiol.* **163**, 637–647.

Grafahrend-Belau, E., Schreiber, F., Koschützki, D. and Junker, B.H. (2009) Flux balance analysis of barley seeds: a computational approach to study systemic properties of central metabolism. *Plant Physiol.* **149**, 585–598.

Graham, I.A. (2008) Seed storage oil mobilization. *Annu. Rev. Plant Biol.* **59**, 115–142.

Grami, B., Baker, R.J. and Stefansson, B.R. (1977) Genetics of protein and oil content in summer rape: heritability, number of effective factors, and correlations. *Can. J. Plant Sci.* **57**, 937–943.

Gu, K., Yi, C., Tian, D., Sangha, J.S., Hong, Y. and Yin, Z. (2012) Expression of fatty acid and lipid biosynthetic genes in developing endosperm of *Jatropha curcas*. *Biotechnol. Biofuels*, **5**, 47.

Ha, J., Shim, S., Lee, T. *et al.* (2019) Genome sequence of *Jatropha curcas* L., a non-edible biodiesel plant, provides a resource to improve seed-related traits. *Plant Biotechnol. J.* **17**, 517–530.

Haferkamp, I. (2007) The diverse members of the mitochondrial carrier family in plants. *FEBS Lett.* **581**, 2375–2379.

Hansen, J. and Møller, I. (1975) Percolation of starch and soluble carbohydrates from plant tissue for quantitative determination with anthrone. *Anal. Biochem.* **68**, 87–94.

Harwood, J.L. (1996) Recent advances in the biosynthesis of plant fatty acids. *Biochim. Biophys. Acta Lipids Lipid Metab.* **1301**, 7–56.

Harwood, J.L. and Guschina, I.A. (2013) Regulation of lipid synthesis in oil crops. *FEBS Lett.*, **587**, 2079–2081.

Harwood, J.L. and Russell, N.J. (1984) Major lipid types in plants and microorganisms. In *Lipids in Plants and Microbes*. Dordrecht: Springer.

Hay, J. and Schwender, J. (2011a) Computational analysis of storage synthesis in developing *Brassica napus* L. (oilseed rape) embryos: flux variability analysis in relation to ^{13}C metabolic flux analysis. *Plant J.* **67**, 513–525.

Hay, J. and Schwender, J. (2011b) Metabolic network reconstruction and flux variability analysis of storage synthesis in developing oilseed rape (*Brassica napus* L.) embryos. *Plant J.* **67**, 526–541.

Hayden, D.M., Rolletschek, H., Borisjuk, L., Corwin, J., Kliebenstein, D.J., Grimberg, A., Stymne, S. and Dehesh, K. (2011) Cofactome analyses reveal enhanced flux of carbon into oil for potential biofuel production. *Plant J.* **67**, 1018–1028.

Holzhütter, H.-G. (2004) The principle of flux minimization and its application to estimate stationary fluxes in metabolic networks. *Eur. J. Biochem.* **271**, 2905–2922.

Huang, A.H.C. (1983) Plant lipases. In *Lipases*. (Brockman, H. and Borgstrom, D., eds). Amsterdam: Elsevier Science Publishers, pp. 419–442.

Igamberdiev, A.U. and Gardeström, P. (2003) Regulation of NAD- and NADP-dependent isocitrate dehydrogenases by reduction levels of pyridine nucleotides in mitochondria and cytosol of pea leaves. *Biochim. Biophys. Acta Bioenerg.* **1606**, 117–125.

Ireland, R.J. and Dennis, D.T. (1981) Isoenzymes of the glycolytic and pentose-phosphate pathways during the development of the castor oil seed. *Can. J. Bot.* **59**, 1423–1425.

Jacquier, N., Mishra, S., Choudhary, V. and Schneiter, R. (2013) Expression of oleosin and perilipins in yeast promotes formation of lipid droplets from the endoplasmic reticulum. *J. Cell Sci.* **126**, 5198–5209.

Jiang, H., Wu, P., Zhang, S. *et al.* (2012) Global analysis of gene expression profiles in developing physic nut (*Jatropha curcas* l.) seeds. *PLoS One*, **7** (5), e36522.

Jiang, W.Z., Henry, I.M., Lynagh, P.G., Comai, L., Cahoon, E.B. and Weeks, D.P. (2017) Significant enhancement of fatty acid composition in seeds of the allohexaploid, *Camelina sativa*, using CRISPR/Cas9 gene editing. *Plant Biotechnol. J.* **15**, 648–657.

Junker, B.H., Lonien, J., Heady, L.E., Rogers, A. and Schwender, J. (2007) Parallel determination of enzyme activities and in vivo fluxes in *Brassica*

napus embryos grown on organic or inorganic nitrogen source. *Phytochemistry*, **68**, 2232–2242.

Kelly, A.A., Shaw, E., Powers, S.J., Kurup, S. and Eastmond, P.J. (2013) Suppression of the *SUGAR-DEPENDENT1* triacylglycerol lipase family during seed development enhances oil yield in oilseed rape (*Brassica napus* L.). *Plant Biotechnol. J.* **11**, 355–361.

Kleczkowski, L.A., Kunz, S. and Wilczynska, M. (2010) Mechanisms of UDP-glucose synthesis in plants. *Crit. Rev. Plant Sci.*, **29**, 191–203.

Krook, J., Vreugdenhil, D., Dijkema, C., van der Plas, L.H.W. (1998) Sucrose and starch metabolism in carrot (*Daucus carota* L.) cell suspensions analysed by ^{13}C-labelling: indications for a cytosol and a plastid-localized oxidative pentose phosphate pathway. *J. Exp. Bot.* **49**, 1917–1924.

Kruger, N.J., Masakapalli, S.K. and Ratcliffe, R.G. (2012) Strategies for investigating the plant metabolic network with steady-state metabolic flux analysis: lessons from an Arabidopsis cell culture and other systems. *J. Exp. Bot.* **63**, 2309–2323.

Lager, I., Glab, B., Eriksson, L., Chen, G., Banas, A. and Stymne, S. (2015) Novel reactions in acyl editing of phosphatidylcholine by lysophosphatidylcholine transacylase (LPCT) and acyl-CoA:glycerophosphocholine acyltransferase (GPCAT) activities in microsomal preparations of plant tissues. *Planta*, **241**, 347–358.

Lakshmanan, M., Lim, S.H., Mohanty, B., Kim, J.K., Ha, S.H. and Lee, D.Y. (2015) Unraveling the light-specific metabolic and regulatory signatures of rice through combined *in silico* modeling and multiomics analysis. *Plant Physiol.* **169**, 3002–3020.

Lands, W.E.M. (1965) Lipid metabolism. *Annu. Rev. Biochem.* **34**, 313–346.

Lee, J., Yun, H., Feist, A.M., Palsson, B. and Lee, S.Y. (2008) Genome-scale reconstruction and in silico analysis of the *Clostridium acetobutylicum* ATCC 824 metabolic network. *Appl. Microbiol. Biotechnol.* **80**, 849–862.

Li-Beisson, Y., Shorrosh, B., Beisson, F. *et al.* (2013) Acyl-lipid metabolism. *Arabidopsis Book*, **11**, e0161.

Li, C., Wang, Y., Liu, L., Hu, Y., Zhang, F., Mergen, S., Wang, G., Schläppi, M.R. and Chu, C. (2011) A rice plastidial nucleotide sugar epimerase is involved in galactolipid biosynthesis and improves photosynthetic efficiency. *PLoS Genet.* **7**, e1002196.

Linka, N. and Weber, A.P.M. (2009) Intracellular metabolite transporters in plants. *Mol. Plant.* **3**, 21–53.

Lisec, J., Schauer, N., Kopka, J., Willmitzer, L. and Fernie, A.R. (2006) Gas chromatography mass spectrometry-based metabolite profiling in plants. *Nat. Protoc.* **1**, 387–396.

Liu, D., Ford, K.L., Roessner, U., Natera, S., Cassin, A.M., Patterson, J.H. and Bacic, A. (2013) Rice suspension cultured cells are evaluated as a model system to study salt responsive networks in plants using a combined proteomic and metabolomic profiling approach. *Proteomics*, **13**, 2046–2062.

Liu, Q., Singh, S.P. and Green, A.G. (2002) High-stearic and high-oleic cottonseed oils produced by hairpin RNA-mediated post-transcriptional gene silencing. *Plant Physiol.* **129**, 1732–1743.

Liu, Q., Wu, M., Zhang, B., Shrestha, P., Petrie, J., Green, A.G. and Singh, S.P. (2017) Genetic enhancement of palmitic acid accumulation in cotton seed oil through RNAi down-regulation of ghKAS2 encoding β-ketoacyl-ACP synthase II (KASII). *Plant Biotechnol. J.* **15**, 132–143.

Lonien, J. and Schwender, J. (2009) Analysis of metabolic flux phenotypes for two Arabidopsis mutants with severe impairment in seed storage lipid synthesis. *Plant Physiol.* **151**, 1617–1634.

Van de Loo, F.J., Broun, P., Turner, S. and Somerville, C. (1995) An oleate 12-hydroxylase from *Ricinus communis* L. is a fatty acyl desaturase homolog. *Proc. Natl Acad. Sci. USA*, **92**, 6743–6747.

Lunn, D., Wallis, J.G. and Browse, J. (2019) Tri-hydroxy-triacylglycerol is efficiently produced by position-specific castor acyltransferases. *Plant Physiol.* **179**, 1050–1063.

Lunn, J.E., Feil, R., Hendriks, J.H.M. *et al.* (2006) Sugar-induced increases in trehalose 6-phosphate are correlated with redox activation of ADPglucose pyrophosphorylase and higher rates of starch synthesis in *Arabidopsis thaliana*. *Biochem. J.* **397**, 139–148.

Luo, B., Groenke, K., Takors, R., Wandrey, C. and Oldiges, M. (2007) Simultaneous determination of multiple intracellular metabolites in glycolysis, pentose phosphate pathway and tricarboxylic acid cycle by liquid chromatography-mass spectrometry. *J. Chromatogr. A*, **1147**, 153–164.

Lv, D., Hu, Z., Lu, L., Lu, H. and Xu, X. (2017) Three-dimensional cell culture: a powerful tool in tumor research and drug discovery. *Oncol. Lett.* **14**, 6999–7010.

Ma, Y., Yin, Z. and Ye, J. (2017) Lipid Biosynthesis and Regulation in Jatropha, an Emerging Model for Woody Energy Plants. *The Jatropha Genome* (Tsuchimoto, S., ed). Cham, Switzerland: Springer International Publishing AG, pp. 112–127.

Maes, W.H., Trabucco, A., Achten, W.M.J. and Muys, B. (2009) Climatic growing conditions of *Jatropha curcas* L. *Biomass Bioenerg.* **33**, 1481–1485.

De Marcos Lousa, C., Roermund, C.W.T.V., Postis, V.L.G., Dietrich, D., Kerr, I.D., Wanders, R.J.A., Baldwin, S.A., Baker, A. and Theodoulou, F.L. (2013) Intrinsic acyl-CoA thioesterase activity of a peroxisomal ATP binding cassette transporter is required for transport and metabolism of fatty acids. *Proc. Natl Acad. Sci. USA*, **110**, 1279–1284.

Di Martino, C.D., Pizzuto, R., Pallotta, M.L., Santis, A.D. and Passarella, S. (2006) Mitochondrial transport in proline catabolism in plants: the existence of two separate translocators in mitochondria isolated from durum wheat seedlings. *Planta*, **223**, 1123–1133.

Masakapalli, S.K., Kruger, N.J. and Ratcliffe, R.G. (2013) The metabolic flux phenotype of heterotrophic Arabidopsis cells reveals a complex response to changes in nitrogen supply. *Plant J.* **74**, 569–582.

Masakapalli, S.K., le Lay, P., Huddleston, J.E., Pollock, N.L., Kruger, N.J. and George Ratcliffe, R. (2010) Subcellular flux analysis of central metabolism in a heterotrophic Arabidopsis cell suspension using steady-state stable isotope labeling. *Plant Physiol.* **152**, 602–619.

Mathews, C., van Holde, K. and Ahern, K. (2002) *Bioquimica* (Salesky, J. ed.) 3rd edn. Buenos Aires, Argentina: Pearson Education S.A.

van de Merbel, A.F., van der Horst, G., van der Mark, M.H., van Uhm, J.I.M., van Gennep, E.J., Kloen, P., Beimers, L., Pelger, R.C.M. and van der Pluijm, G. (2018) An *ex vivo* tissue culture model for the assessment of individualized drug responses in prostate and bladder cancer. *Front. Oncol.* **8**, 400.

Miernyk, J.A. and Dennis, D.T. (1992) A developmental analysis of the enolase isozymes from *Ricinus communis*. *Plant Physiol.* **99**, 748–750.

Miernyk, J.A. and Dennis, D.T. (1982) Isozymes of the glycolytic enzymes in endosperm from developing castor oil seeds. *Plant Physiol.* **69**, 825–828.

Millard, P., Letisse, F., Sokol, S. and Portais, J.C. (2012) IsoCor: correcting MS data in isotope labeling experiments. *Bioinformatics*, **28**, 1294–1296.

Mintz-Oron, S., Meir, S., Malitsky, S., Ruppin, E., Aharoni, A. and Shlomi, T. (2012) Reconstruction of Arabidopsis metabolic network models accounting for subcellular compartmentalization and tissue-specificity. *Proc. Natl Acad. Sci. USA*, **109**, 339–344.

Monaco, M.K., Sen, T.Z., Dharmawardhana, P.D. *et al.* (2013) Maize metabolic network construction and transcriptome analysis. *Plant Genome*, **6**, 1–2.

Montes, J.M. and Melchinger, A.E. (2016) Domestication and breeding of *Jatropha curcas* L. *Trends Plant Sci.* **21**, 1045–1057.

Moreira, T.B., Shaw, R., Luo, X. *et al.* (2019) A genome-scale metabolic model of soybean (*Glycine max*) highlights metabolic fluxes in seedlings. *Plant Physiol.* **180**, 1912–1929.

Morineau, C., Bellec, Y., Tellier, F., Gissot, L., Kelemen, Z., Nogué, F. and Faure, J.-D. (2017) Selective gene dosage by CRISPR-Cas9 genome editing in hexaploid *Camelina sativa*. *Plant Biotechnol. J.* **15**, 729–739.

Napier, J.A. (2007) The production of unusual fatty acids in transgenic plants. *Annu. Rev. Plant Biol.* **58**, 295–319.

Napier, J.A. and Graham, I.A. (2010) Tailoring plant lipid composition: designer oilseeds come of age. *Curr. Opin. Plant Biol.* **13**, 329–336.

Napier, J.A., Haslam, R.P., Beaudoin, F. and Cahoon, E.B. (2014) Understanding and manipulating plant lipid composition: metabolic engineering leads the way. *Curr. Opin. Plant Biol.* **19**, 68–75.

Nash, T. (1953) The colorimetric estimation of formaldehyde by means of the Hantzsch reaction. *Biochem. J.* **55**, 416–421.

Nielsen, J., Villadsen, J. and Lidén, G. (2003) Modeling of Growth Kinetics. In *Bioreaction Engineering Principles*. New York: Springer Science+Business Media, LLC, 2nd edn, pp. 1–8.

Nikoloski, Z., Perez-Storey, R. and Sweetlove, L.J. (2015) Inference and prediction of metabolic network fluxes. *Plant Physiol.* **169**, 1443–1455.

Parthibane, V., Rajakumari, S., Venkateshwari, V., Iyappan, R. and Rajasekharan, R. (2012) Oleosin is bifunctional enzyme that has both monoacylglycerol acyltransferase and phospholipase activities. *J. Biol. Chem.* **287**, 1946–1954.

Pfau, T., Christian, N., Masakapalli, S.K., Sweetlove, L.J., Poolman, M.G. and Ebenhöh, O. (2018) The intertwined metabolism during symbiotic nitrogen fixation elucidated by metabolic modelling. *Sci. Rep.* **8**, 1–11.

Pilalis, E., Chatziioannou, A., Thomasset, B. and Kolisis, F. (2011) An *in silico* compartmentalized metabolic model of *Brassica napus* enables the systemic study of regulatory aspects of plant central metabolism. *Biotechnol. Bioeng.* **108**, 1673–1682.

Planchais, S., Cabassa, C., Toka, I., Justin, A.-M., Renou, J.-P., Savouré, A. and Carol, P. (2014) BASIC AMINO ACID CARRIER 2 gene expression modulates arginine and urea content and stress recovery in Arabidopsis leaves. *Front. Plant Sci.* **5**, 330.

Pleite, R., Pike, M.J., Garcés, R., Martínez-Force, E. and Rawsthorne, S. (2005) The sources of carbon and reducing power for fatty acid synthesis in the heterotrophic plastids of developing sunflower (*Helianthus annuus* L.) embryos. *J. Exp. Bot.* **56**, 1297–1303.

Poirier, Y., Ventre, G. and Caldelari, D. (1999) Increased flow of fatty acids toward β-oxidation in developing seeds of Arabidopsis deficient in diacylglycerol acyltransferase activity or synthesizing medium-chain-length fatty acids. *Plant Physiol.* **121**, 1359–1366.

Pollard, M., Delamarter, D., Martin, T.M. and Shachar-Hill, Y. (2015a) Lipid labeling from acetate or glycerol in cultured embryos of *Camelina sativa* seeds: a tale of two substrates. *Phytochemistry*, **118**, 192–203.

Pollard, M., Martin, T.M. and Shachar-Hill, Y. (2015b) Lipid analysis of developing *Camelina sativa* seeds and cultured embryos. *Phytochemistry*, **118**, 23–32.

Ponce-de-León, M., Montero, F. and Peretó, J. (2013) Solving gap metabolites and blocked reactions in genome-scale models: application to the metabolic network of *Blattabacterium cuenoti*. *BMC Syst. Biol.* **7**, 114.

Poolman, M.G., Kundu, S., Shaw, R. and Fell, D.A. (2013) Responses to light intensity in a genome-scale model of rice metabolism. *Plant Physiol.* **162**, 1060–1072.

Poolman, M.G., Miguet, L., Sweetlove, L.J. and Fell, D.A. (2009) A genome-scale metabolic model of Arabidopsis and some of its properties. *Plant Physiol.* **151**, 1570–1581.

Quettier, A.L. and Eastmond, P.J. (2009) Storage oil hydrolysis during early seedling growth. *Plant Physiol. Biochem.* **47**, 485–490.

Radrich, K., Tsuruoka, Y., Dobson, P., Gevorgyan, A., Swainston, N., Baart, G. and Schwartz, J.M. (2010) Integration of metabolic databases for the reconstruction of genome-scale metabolic networks. *BMC Syst. Biol.* **4**, 114.

Van der Rest, B.V., Boisson, A.M., Gout, E., Bligny, R. and Douce, R. (2002) Glycerophosphocholine metabolism in higher plant cells. Evidence of a new glyceryl-phosphodiester phosphodiesterase. *Plant Physiol.* **130**, 244–255.

Reynolds, K.B., Taylor, M.C., Cullerne, D.P., Blanchard, C.L., Wood, C.C., Singh, S.P. and Petrie, J.R. (2017) A reconfigured Kennedy pathway which promotes efficient accumulation of medium-chain fatty acids in leaf oils. *Plant Biotechnol. J.* **15**, 1397–1408.

Reynolds, K.B., Taylor, M.C., Zhou, X.-R., Vanhercke, T., Wood, C.C., Blanchard, C.L., Singh, S.P. and Petrie, J.R. (2015) Metabolic engineering of medium-chain fatty acid biosynthesis in *Nicotiana benthamiana* plant leaf lipids. *Front. Plant Sci.* **6**, 164.

Rontein, D., Dieuaide-Noubhani, M., Dufourc, E.J., Raymond, P. and Rolin, D. (2002) The metabolic architecture of plant cells: stability of central metabolism and flexibility of anabolic pathways during the growth cycle of tomato cells. *J. Biol. Chem.* **277**, 43948–43960.

Rossi, M.T., Kalde, M., Srisakvarakul, C., Kruger, N.J. and George Ratcliffe, R. (2017) Cell-type specific metabolic flux analysis: a challenge for metabolic phenotyping and a potential solution in plants. *Metabolites*, **7**, 59.

Saha, R., Suthers, P.F. and Maranas, C.D. (2011) *Zea mays* iRS1563: a comprehensive genome-scale metabolic reconstruction of maize metabolism. *PLoS One*, **6**, e21784.

Salem, M.A., Jüppner, J., Bajdzienko, K. and Giavalisco, P. (2016) Protocol: a fast, comprehensive and reproducible one-step extraction method for the rapid preparation of polar and semi-polar metabolites, lipids, proteins, starch and cell wall polymers from a single sample. *Plant Methods*, **12**, 45.

Samal, A. (2008) Conservation of high-flux backbone in alternate optimal and near-optimal flux distributions of metabolic networks. *Syst. Synth. Biol.* **2**, 83–93.

Schellenberger, J., Que, R., Fleming, R.M.T. *et al.* (2011) Quantitative prediction of cellular metabolism with constraint-based models: the COBRA Toolbox v2.0. *Nat. Protoc.* **6**, 1290–1307.

Schwender, J., Goffman, F., Ohlrogge, J.B. and Shachar-Hill, Y. (2004) Rubisco without the Calvin cycle improves the carbon efficiency of developing green seeds. *Nature*, **432**, 779–782.

Schwender, J. and Hay, J.O. (2012) Predictive modeling of biomass component tradeoffs in *Brassica napus* developing oilseeds based on *in silico* manipulation of storage metabolism. *Plant Physiol.* **160**, 1218–1236.

Schwender, J., Hebbelmann, I., Heinzel, N. *et al.* (2015) Quantitative multilevel analysis of central metabolism in developing oilseeds of oilseed rape during *in vitro* culture. *Plant Physiol.* **168**, 828–848.

Schwender, J. and Ohlrogge, J.B. (2002) Probing in vivo metabolism by stable isotope labeling of storage lipids and proteins in developing *Brassica napus* embryos. *Plant Physiol.* **130**, 347–361.

Schwender, J., Shachar-Hill, Y. and Ohlrogge, J.B. (2006) Mitochondrial metabolism in developing embryos of *Brassica napus*. *J. Biol. Chem.* **281**, 34040–34047.

Seaver, S.M.D., Bradbury, L.M.T., Frelin, O., Zarecki, R., Ruppin, E., Hanson, A.D. and Henry, C.S. (2015) Improved evidence-based genome-scale metabolic models for maize leaf, embryo, and endosperm. *Front. Plant Sci.* **6**, 142.

Shaw, R. and Cheung, C.Y.M. (2018) A dynamic multi-tissue flux balance model captures carbon and nitrogen metabolism and optimal resource partitioning during Arabidopsis growth. *Front. Plant Sci.* **9**, 884.

Shindou, H. and Shimizu, T. (2009) Acyl-CoA:lysophospholipid acyltransferases. *J. Biol. Chem.* **284**, 1–5.

Siloto, R.M.P., Findlay, K., Lopez-Villalobos, A., Yeung, E.C., Nykiforuk, C.L. and Moloney, M.M. (2006) The accumulation of oleosins determines the size of seed oilbodies in Arabidopsis. *Plant Cell*, **18**, 1961–1974.

Simons, M., Saha, R., Amiour, N. *et al.* (2014) Assessing the metabolic impact of nitrogen availability using a compartmentalized maize leaf genome-scale model. *Plant Physiol.* **166**, 1659–1674.

Slack, C.R., Campbell, L.C., Browse, J.A. and Roughan, P.G. (1983) Some evidence for the reversibility of the cholinephosphotransferase-catalysed reaction in developing linseed cotyledons *in vivo* [*Linum usitatissimum*]. *Biochim. Biophys. Acta Lipids Metab.* **754**(1), 10–20.

Slack, C.R., Roughan, P.G. and Balasingham, N. (1978) Labelling of glycerolipids in the cotyledons of developing oilseeds by [1-^{14}C]acetate and [2-^{3}H]glycerol. *Biochem. J.* **170**, 421–433.

Somani, B.L., Khanade, J. and Sinha, R. (1987) A modified anthrone-sulfuric acid method for the determination of fructose in the presence of certain proteins. *Anal. Biochem.* **167**, 327–330.

Sood, A. and Chauhan, R.S. (2015) Regulation of FA and TAG biosynthesis pathway genes in endosperms and embryos of high and low oil content genotypes of *Jatropha curcas* L. *Plant Physiol. Biochem.* **94**, 253–267.

Speerling, P. and Heinz, E. (1993) Isomeric sn-1-octadecenyl and sn-2-octadecenyl analogues of lysophosphatidylcholine as substrates for acylation and desaturation by plant microsomal membranes. *Eur. J. Biochem.* **213**, 965–971.

Sperling, P., Linscheid, M., Stocker, S., Muhlbach, H.P. and Heinz, E. (1993) *In vivo* desaturation of cis-Δ9-monounsaturated to cis-Δ9,12- diunsaturated alkenylether glycerolipids. *J. Biol. Chem.* **268**, 26935–26940.

Sriram, G., Fulton, D.B., Iyer, V.V., Peterson, J.M., Zhou, R., Westgate, M.E., Spalding, M.H. and Shanks, J.V. (2004) Quantification of compartmented metabolic fluxes in developing soybean embryos by employing biosynthetically directed fractional ^{13}C labeling, two-dimensional [^{13}C, ^{1}H] nuclear magnetic resonance, and comprehensive isotopomer balancing. *Plant Physiol.* **136**, 3043–3057.

Stoutjesdijk, P.A., Hurlestone, C., Singh, S.P. and Green, A.G. (2000) High-oleic acid Australian *Brassica napus* and *B. juncea* varieties produced by co-suppression of endogenous Delta12-desaturases. *Biochem. Soc. Trans.* **28**, 938–940.

Stymne, S. and Stobart, A.K. (1984) Evidence for the reversibility of the acyl-CoA:lysophosphatidylcholine acyltransferase in microsomal preparations from developing safflower (*Carthamus tinctorius* L.) cotyledons and rat liver. *Biochem. J.* **223**, 305–314.

Stymne, S. and Stobart, A.K. (1987) Triacylglycerol biosynthesis. In *The Biochemistry of Plants: A Comprehensive Treatise, Volume 9: Lipids: Structure and Function* (Stumpf, P.K., ed). New York: Academic Press, pp. 175–214.

Sweetlove, L.J. and George Ratcliffe, R. (2011) Flux-balance modeling of plant metabolism. *Front. Plant Sci.* **2**, 38.

Sweetlove, L.J., Williams, T.C.R., Cheung, C.Y.M. and Ratcliffe, R.G. (2013) Modelling metabolic CO_2 evolution – a fresh perspective on respiration. *Plant. Cell Environ.* **36**, 1631–1640.

Tahchy, A.E., Reynolds, K.B., Petrie, J.R., Singh, S.P. and Vanhercke, T. (2017) Thioesterase overexpression in *Nicotiana benthamiana* leaf increases the fatty acid flux into triacylgycerol. *FEBS Lett.* **591**, 448–456.

Thelen, J.J. and Ohlrogge, J.J. (2002) Metabolic engineering of fatty acid biosynthesis in plants. *Metab. Eng.* **4**, 12–21.

Theodoulou, F.L. and Eastmond, P.J. (2012) Seed storage oil catabolism: a story of give and take. *Curr. Opin. Plant Biol.* **15**, 322–328.

Thiele, I. and Palsson, B. (2010) A protocol for generating a high-quality genome-scale metabolic reconstruction. *Nat. Protoc.* **5**, 93–121.

Triki, S., Demandre, C. and Mazliak, P. (1999) Biosynthesis of triacylglycerols by developing sunflower seed microsomes. *Phytochemistry*, **52**, 55–62.

Vanhercke, T., Divi, U.K., Tahchy, A.E. *et al.* (2017) Step changes in leaf oil accumulation via iterative metabolic engineering. *Metab. Eng.* **39**, 237–246.

Varma, A. and Palsson, B.O. (1994) Stoichiometric flux balance models quantitatively predict growth and metabolic by-product secretion in wild-type *Escherichia coli* W3110. *Appl. Environ. Microbiol.* **60**, 3724–3731.

Watanabe, M., Tohge, T., Balazadeh, S., Erban, A., Giavalisco, P., Kopka, J., Mueller-Roeber, B., Fernie, A.R. and Hoefgen, R. (2018) Comprehensive metabolomics studies of plant developmental senescence. In *Plant Senescence. Methods and Protocols* (Guo, Y., ed). New York, NY: Humana Press Inc., pp. 339–358.

Wiechert, W. (2001) ^{13}C metabolic flux analysis. *Metab. Eng.* **3**, 195–206.

Williams, T.C.R., Miguet, L., Masakapalli, S.K., Kruger, N.J., Sweetlove, L.J. and Ratcliffe, R.G. (2008) Metabolic network fluxes in heterotrophic Arabidopsis cells: stability of the flux distribution under different oxygenation conditions. *Plant Physiol.* **148**, 704–718.

Williams, T.C.R., Poolman, M.G., Howden, A.J.M., Schwarzlander, M., Fell, D.A., Ratcliffe, R.G. and Sweetlove, L.J. (2010) A genome-scale metabolic model accurately predicts fluxes in central carbon metabolism under stress conditions. *Plant Physiol.* **154**, 311–323.

Winichayakul, S., William Scott, R., Roldan, M., Bertrand Hatier, J.H., Livingston, S., Cookson, R., Curran, A.C. and Roberts, N.J. (2013) *In vivo* packaging of triacylglycerols enhances Arabidopsis leaf biomass and energy density. *Plant Physiol.* **162**, 626–639.

Woese, C.R., Olsen, G.J., Ibba, M. and Soll, D. (2000) Aminoacyl-tRNA synthetases, the genetic code, and the evolutionary process. *Microbiol. Mol. Biol. Rev.* **64**, 202–236.

Xu, R., Wang, R. and Liu, A. (2011) Expression profiles of genes involved in fatty acid and triacylglycerol synthesis in developing seeds of Jatropha (*Jatropha curcas* L.). *Biomass Bioenerg.* **35**, 1683–1692.

Xu, X., Vanhercke, T., Shrestha, P. *et al.* (2019) Upregulated lipid biosynthesis at the expense of starch production in potato (*Solanum tuberosum*) vegetative tissues via simultaneous downregulation of ADP-glucose pyrophosphorylase and sugar dependent1 expressions. *Front. Plant Sci.* **10**, 1444.

Yuan, H., Cheung, M.C.Y., Poolman, M.G., Hilbers, P.A.J. and van Riel, N.A.W. (2016) A genome-scale metabolic network reconstruction of tomato (*Solanum lycopersicum* L.) and its application to photorespiratory metabolism. *Plant J.* **85**, 289–304.

Yuan, J., Bennett, B.D. and Rabinowitz, J.D. (2008) Kinetic flux profiling for quantitation of cellular metabolic fluxes. *Nat. Protoc.* **3**, 1328–1340.

Yuan, L. and Grotewold, E. (2015) Metabolic engineering to enhance the value of plants as green factories. *Metab. Eng.* **27**, 83–91.

Zhang, H., Wu, C., Wu, Q., Dai, J. and Song, Y. (2016) Metabolic flux analysis of lipid biosynthesis in the yeast *Yarrowia lipolytica* using ^{13}C-labled glucose and gas chromatography-mass spectrometry. *PLoS One*, **11**, e0159187.

Zhang, M., Fan, J., Taylor, D.C. and Ohlrogge, J.B. (2009) DGAT1 and PDAT1 acyltransferases have overlapping functions in Arabidopsis triacylglycerol biosynthesis and are essential for normal pollen and seed development. *Plant Cell*, **21**, 3885–3901.